contract with them. The unit was pulled with a spring balance. In the measurement of the rotation support force, a unit was set up under the same conditions as for measuring vertical support force, and turned. Table 6.2 lists the experimental results. The vertical suppo s rt force in the launcher was set to 100 N to maintain body position. This can be achieved with one contracted unit—balancing the robot weight and a pushing force of 55 N. The force in the soil was 32 N, therefore at least two units are needed to maintain body position. The maximum rotation reaction capacity in a launcher was 7 Nm and that in soil was estimated as 4.8 Nm. The maximum rotation action force of the excavation unit was about 18 Nm in the experiments conducted with the excavation unit. As such,

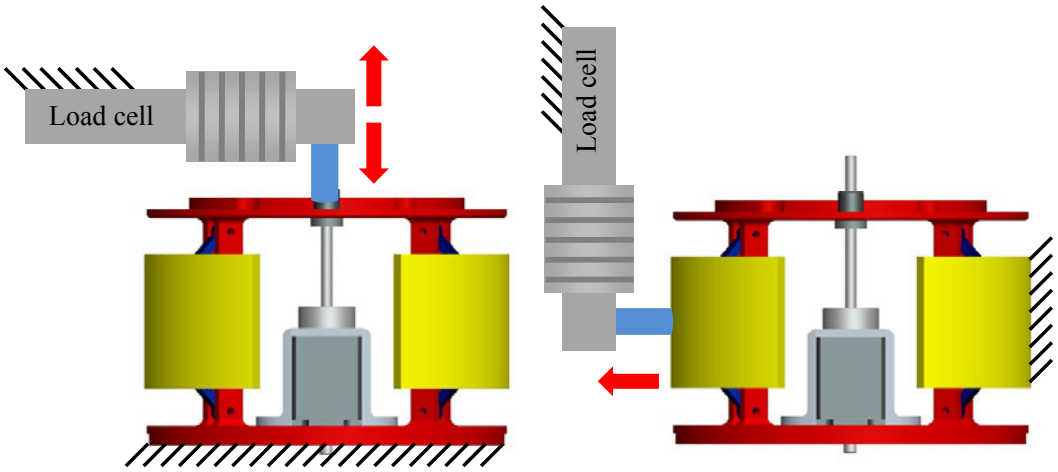


a) Contraction and extension force b) Expansion force

Fig. 6.11 Subunit force experiments

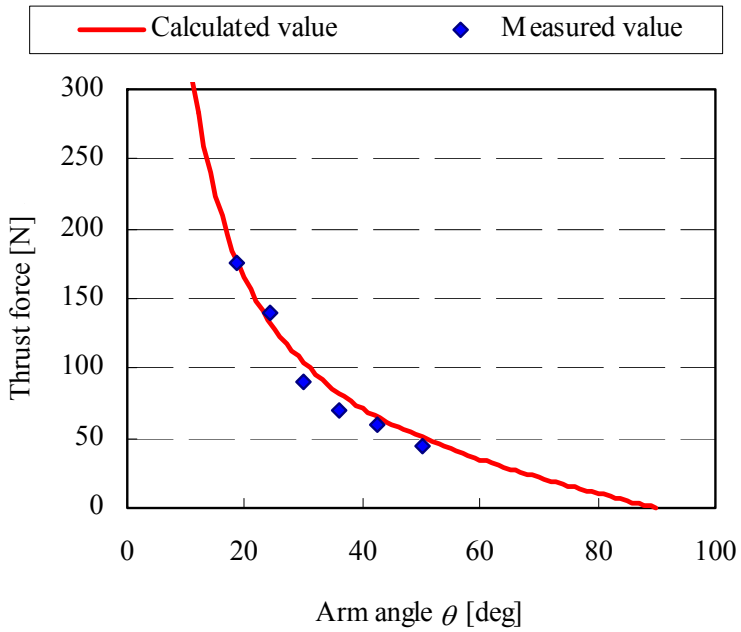


Fig. 6.12 Expansion force of a unit

the device does not meet the requirements. However, possible improvements are as follows: different materials for expansion plates, surfaces with tiny projections, using another actuator and increased area of the launcher could make it work properly, both inside the launcher and in the soil.

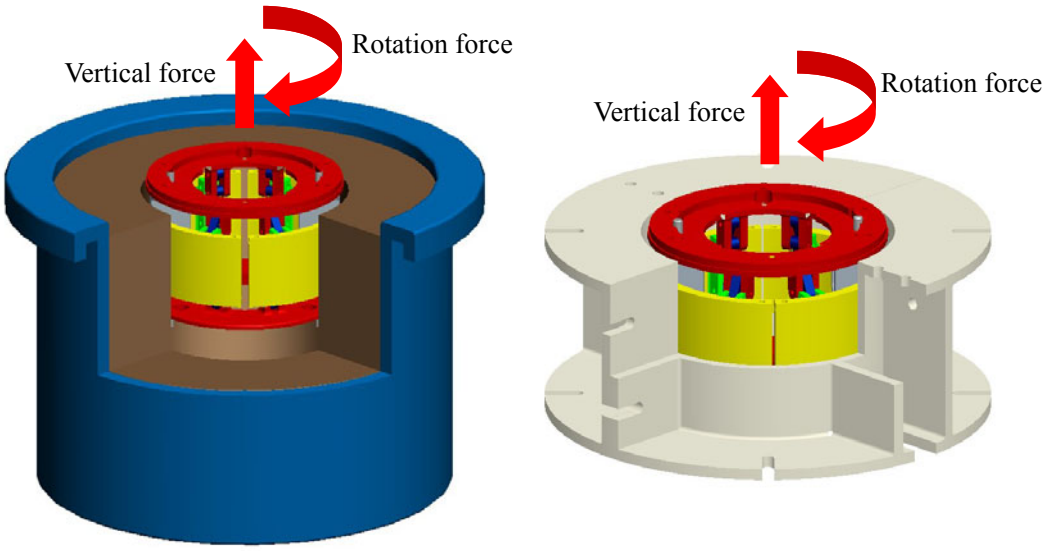


a) Inside soil b) Inside a launcher

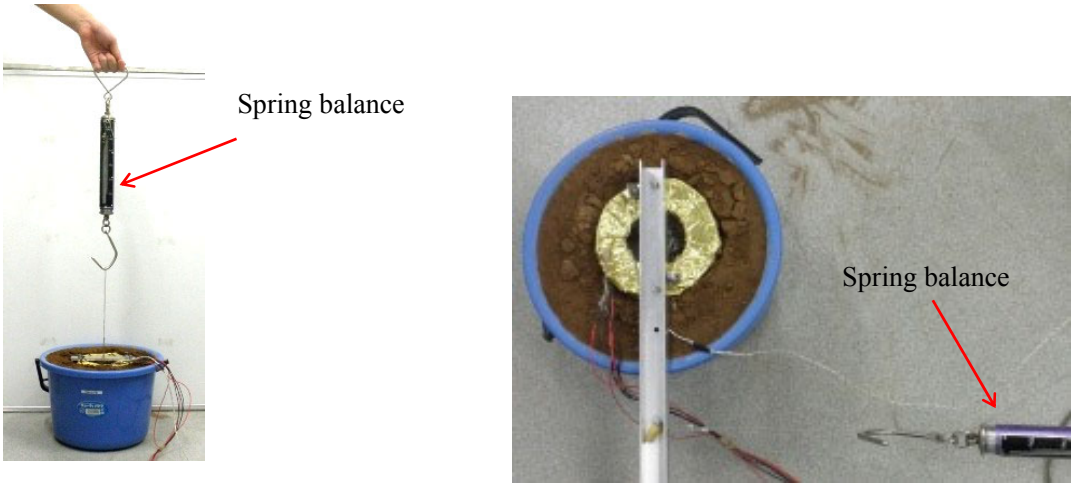


a) Measurement of vertical force b) Measurement of rotational friction force in soil

Fig. 6.13 Measurement of vertical and rotation support force

Table 6.2 Experimental results in a launcher and soil

| | Launcher | Soil |
|---|---|---|
| Rotation reaction [Nm] | 7 | 4.8 |
| Vertical support force [N] | 100 | 32 |

# Chapter 7: Development of a Subsurface Explorer

This section describes the development of a prototype of a subsurface explorer, which improves upon the previous individual designs and integrates the two units.

## 7.1 Prototype robot Integrating Propulsion and Excavation Units

Fig. 7.1 and Fig. 7.2 show the excavation and propulsion units, combining both units into the developed robot. It consists of four propulsion rings, each of which has four expansion plates.

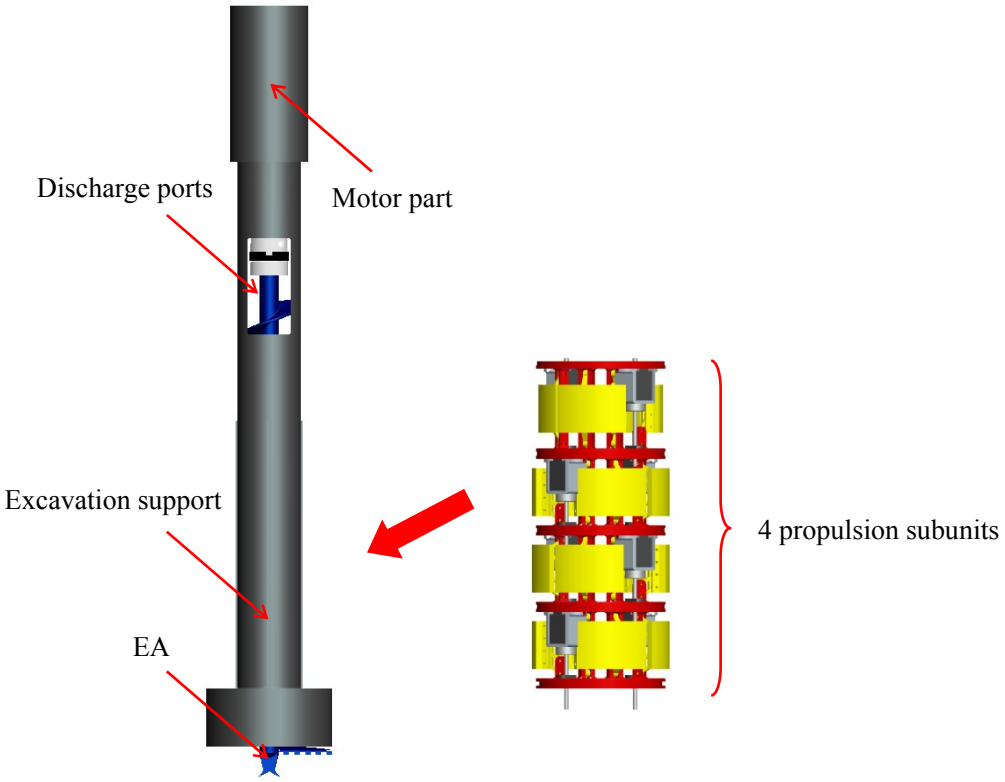


Fig. 7.1 Excavation and propulsion units for combination

Additional rubber friction sheets are placed on the outer surface of the expansion plates, which increase the friction forces while the robot is moving inside a launcher. These plates cover a large area of the outer surface of the unit. The remaining uncovered spaces, i.e., the gaps between the propulsion units and those between the expansion plates, are covered with dustproof material (aluminium evaporation sheets) to prevent soil from getting inside the rings. These sheets are positioned so as not to hinder the contraction and extension of the unit. The excavation unit is connected to the front of the propulsion unit, and the transport part passes through, inside the propulsion rings. A DC motor located at the rear end of the robot powers the EA. The excavated soil is discharged from discharge ports behind the propulsion unit. The total mass of the prototype robot is 5.28 kg and its length is 800 mm.

The excavation depth in terms of the lateral earth pressure is calculated using the equation (2.5) – (2.7). A propulsion subunit contracts and expands in radial direction. The contracted subunit theoretically does not touch the surface of the wall and suffer from the earth pressure from the wall. On the other hand, the front part of the excavation unit contacts with the wall. For calculation, some parameters were taken from Table 5.5. The length of contact area of the robot is $H_L$ = 0.06 mm. Fig 7.3 shows the depth prediction of the robot and excavation unit, calculated with the weight of the robot in the horizontal axis and depth in the vertical. It is seen that the robot can move deeper than the excavation unit alone with the same weight. The propulsion unit can generate the pushing force of 55 N. The cross point between 55 N and the depth of the robot, which is 7.7 m, indicates the

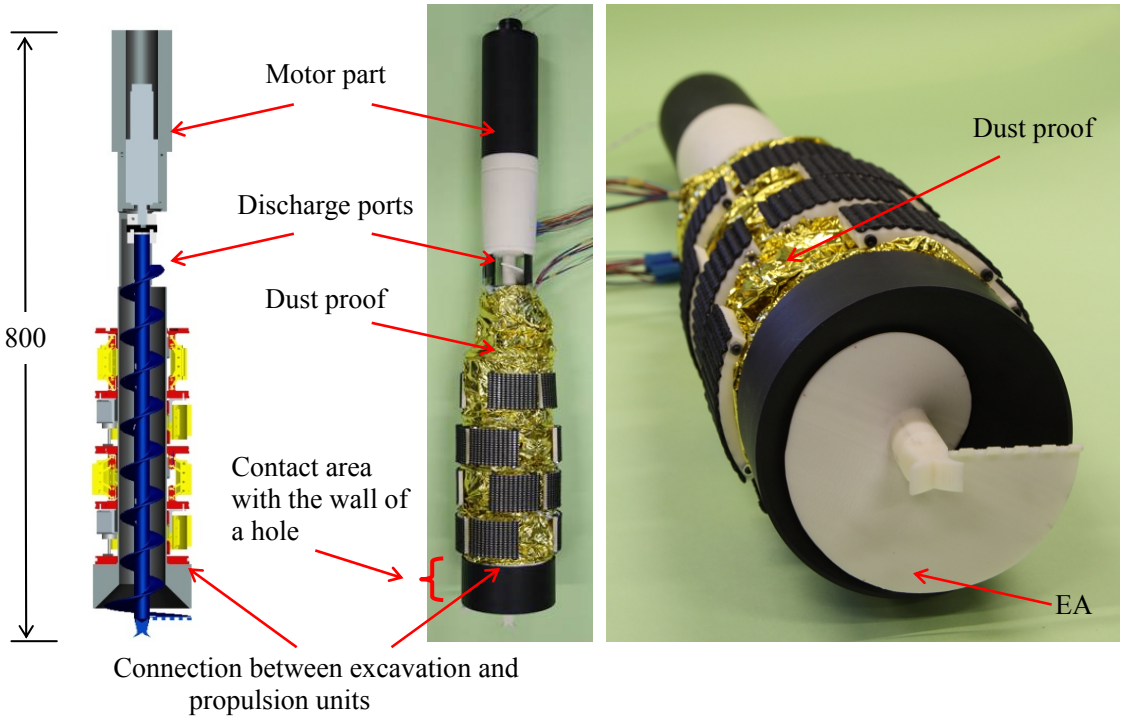


Fig. 7.2 Developed robot with excavation and propulsion units

reachable depth of the robot in terms of the earth pressure preventing excavation.

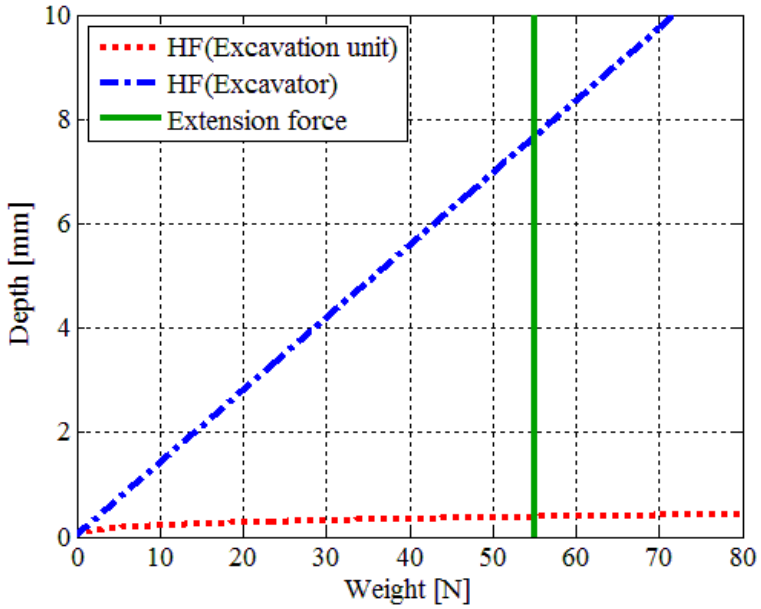


Fig. 7.3 Depth prediction of the robot and excavation unit

## 7.2 Control System

The control system was made as functional yet as simple as possible for the prototype robot. A design for use in an actual mission in space in terms of robustness of implementation is a possible future extension of the project. In the experiments, the excavation and propulsion units are controlled in a distributed way, each including their respective resources. For the excavation unit, a computer (PC) controls the DC motor via a motor driver. The motor rotates at a constant speed with the feedback data received from an encoder. The PC also monitors the current level, which is approximately proportional to the motor torque. In the propulsion units, an H8 microcontroller controls the stepper motors.

## 7.3 Propulsion Velocity

Altering the extension or contraction phases of each unit can achieve several motion patterns of the robot. Fig. 7.4 illustrates the definition of motion pattern of the peristaltic crawling. Motion patterns consist of a wavelength, propagation speed and number of waves. Here, wavelength is defined as the number of units extended in the axial direction. The propagation speed is the number of contracted subunits propagated in the rear. The number of waves is the number of adjacent contracted subunits. The basic motion patterns are identified as an *l*–*s*–*n* motion (wavelength - propagation speed -

number of waves). The developed robot includes 4 subunits, and it uses the pattern 1-1-1, which is depicted in the yellow propulsion unit of Fig. 7.4.

The extension speed of a unit $v$ is given as follows:

$$v = \frac{dP}{Pt} \tag{7.1}$$

Here the top plate of a subunit moves a $d$ (μm) distance when a pulse signal is sent to stepper motors. $P$ is the number of pulse signals from the H8 microcontroller. The time $t$ (μs) is the cycle length of a pulse signal.

Then propulsion speed $V$ (mm/s) is given as follows:

$$V = v\frac{l}{N} = \frac{dl}{Nt} \tag{7.2}$$

Here $N$ is the total number of subunits, 4 for this robot. The robot moves with a 1-1-1 pattern and moves forward by the difference of contraction and extension of one subunit. $l$ is multiplied to $v$ because it is the number of subunits simultaneously extended. $v$ is divided by $N$ because the robot moves forward once in a cycle of $N$ motions.

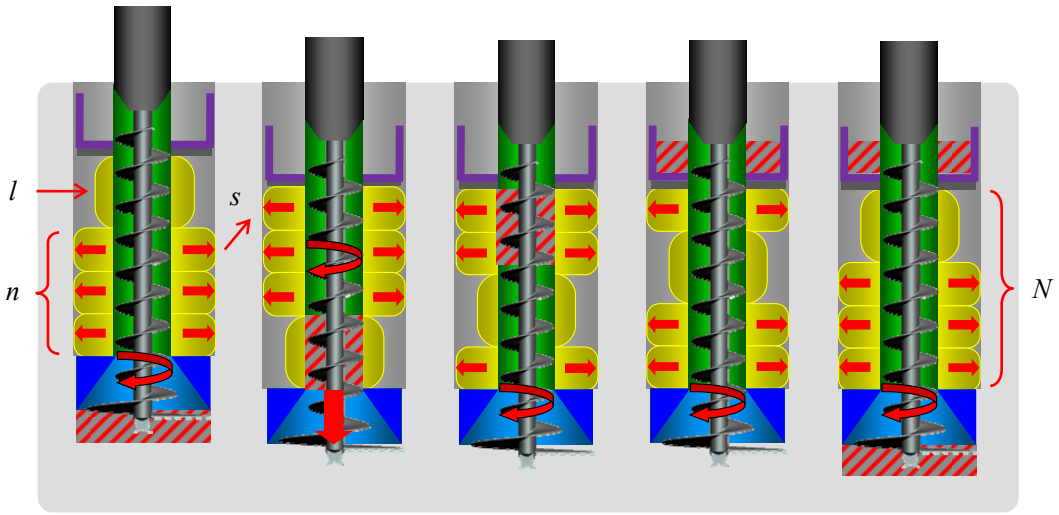


Wavelength ($l$): Number of subunits extended in axial direction;
Propagation Speed ($s$): Number of contracted subunits propagated in the rear;
Number of waves ($n$): Number of adjacent contracted subunits.
Total number of subunits ($N$)

Fig. 7.4 Definition of motion pattern

## 7.4 Propulsion Experiments in a Pipe

The downward propulsion velocity $V$ is compared in (7.2) with its experimented equivalent in a pipe. The 1-1-1 propulsion pattern was used for this experiment. Marks were placed in the middle of

each unit and analysed using a motion analysis software (MOVIAS Pro, Nac Image Technology Inc.). Target velocities were set at 0.5 and 1.0 mm/s values.

The tracks of marks are shown in Fig. 7.5 for a speed of 1.0 mm/s. The front subunit first contracts, then this contraction propagates to the rear subunit in the same fashion as a natural, living earthworm does in Fig. 3.4. Table 7.1 shows experimental and calculated velocities. Slight differences are visible, nevertheless it can be concluded that the robot moves as planned.

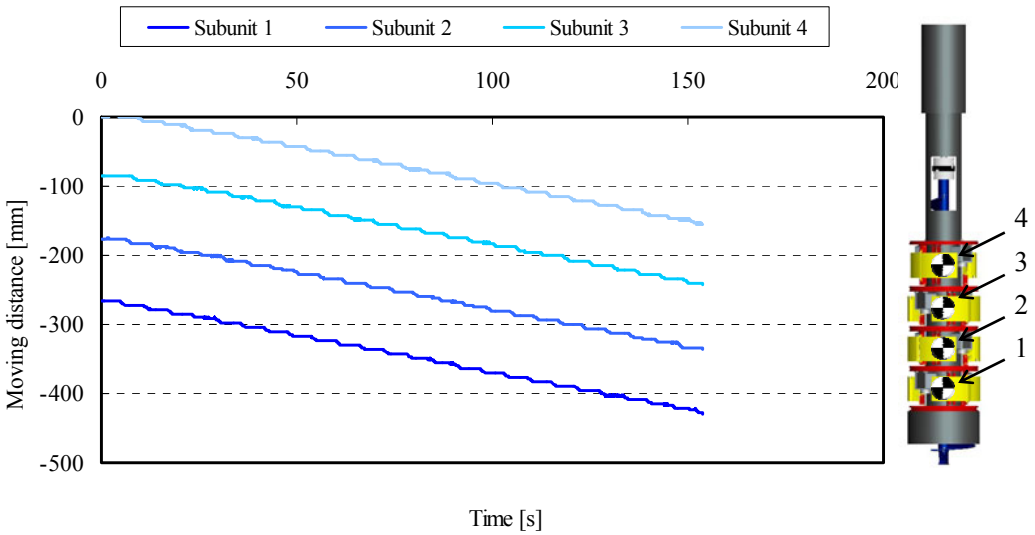


Fig. 7.5 Movement tracks of the propulsion unit

Table 7.1 Velocity comparisons

| Desired velocity [mm/s] | Theoretical velocity [mm/s] | Experimental velocity [mm/s] |
|---|---|---|
| 0.50 | 0.50 | 0.47 |
| 1.00 | 1.00 | 1.06 |

# 7.5 Excavation Experiments

### 7.5.1 Experimental Setup

Fig. 7.6 shows the experimental excavation setup for the developed robot. The launcher, which supports peristaltic crawling until the robot reaches the soil, would be installed on a rover in an actual mission. The launcher is made of ABS and has three stages, covering three rings of the propulsion unit from the front. The robot is able to move using peristaltic crawling, but needs at least three units to generate this kind of locomotion. Each stage can be separated to avoid covering the discharge ports of the robot. In this experiment, the rotation speed of the EA was set at 10 r/min. A 1-1-1 propulsion pattern was used, and the ring extension velocity was set at 1.0 mm/s. The robot velocity is 0.25 mm/s as validated in an earlier section. Here, the depth of excavation is measured

from the wire sensor, and motor torque is measured from the current output of the motor driver. The experiments continued until the discharge ports reached soil level.

For possible future missions, the excavator could operate on the Moon or other bodies with a gravity six times less intense than that of the Earth. The developed device has been tested for excavation experiments in similar, lighter weight conditions by using counterweights. The forces applied to the EA were set at 1/1, 1/2 (26 N), 1/4 (13 N) and 1/6 (8.7 N) of its own weight on Earth of 52 N.

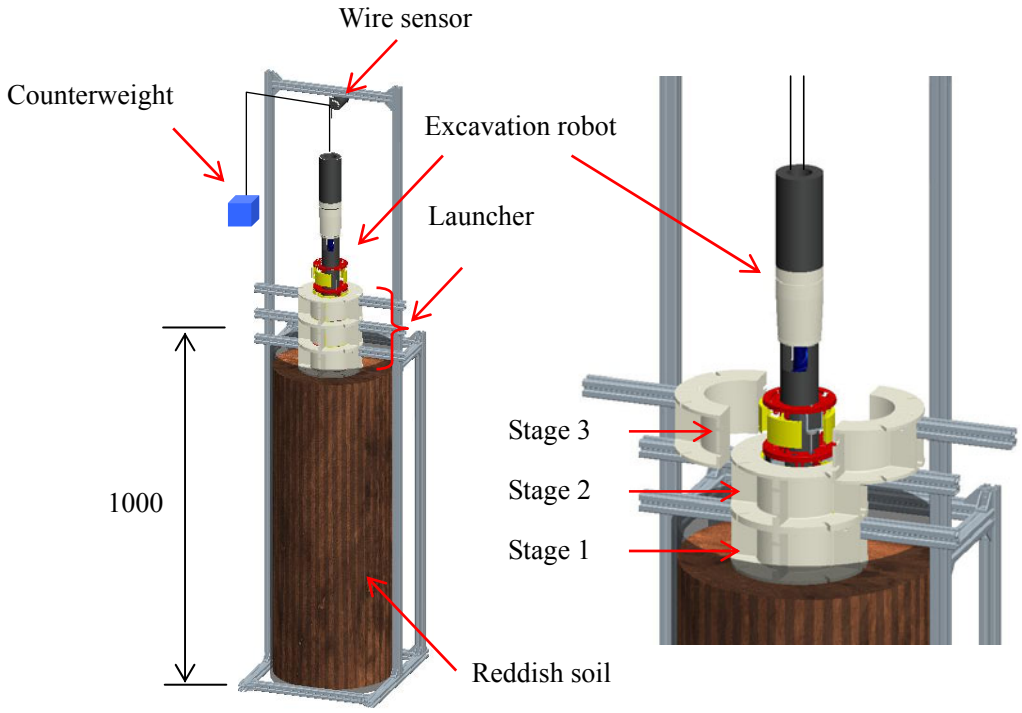


Fig. 7.6 Experimental setup

### 7.5.2 Experimental Results for Various Excavation Conditions

Fig. 7.7 shows the experimental process. This process can be described in six phases, as given in the following.

1) Beginning of the experiment.
2) Discharge ports reaching Stage 3.
3) Stage 3 of the launcher separated to both sides.
4) After Stage 2 separation.
5) After Stage 1 separation.
6) Excavation stopped when discharged ports reached soil level.

Fig. 7.8 shows the experimental results in terms of depth of excavation and motor torque as functions of time. As shown in this figure, the excavation velocity mainly changed at approximately 9 min when the robot was released from the top stage of the launcher. Then, for 1 or 2 minutes, the velocity became faster than that prior to the 9-min mark. The motor torque also increased because of this slip. At this point, the front ring was moving in the soil and the other rings were moving in the launcher. It assumes that it was difficult to generate enough friction force because the surface of shallow soil was weak and not packed. Excavation remained constant until the bottom stage of the launcher was released. From this point on, the robot continued excavating although the velocity decreased. The hole and the robot were investigated after excavation. It seemed that the discharged soil then fell into the hole, preventing the propulsion unit from working properly. The experimental results for the excavation unit alone appear to be almost straight in Fig. 5.18. In contrast, the results for the new robot, with both units integrated, clearly depict a stair shape in Fig. 7.5, and the robot did not just fall down through the hole under its own weight, but succeeded in moving using peristaltic crawling. The robot could excavate to a depth of 430 mm, i.e., deeper than the excavation unit alone.

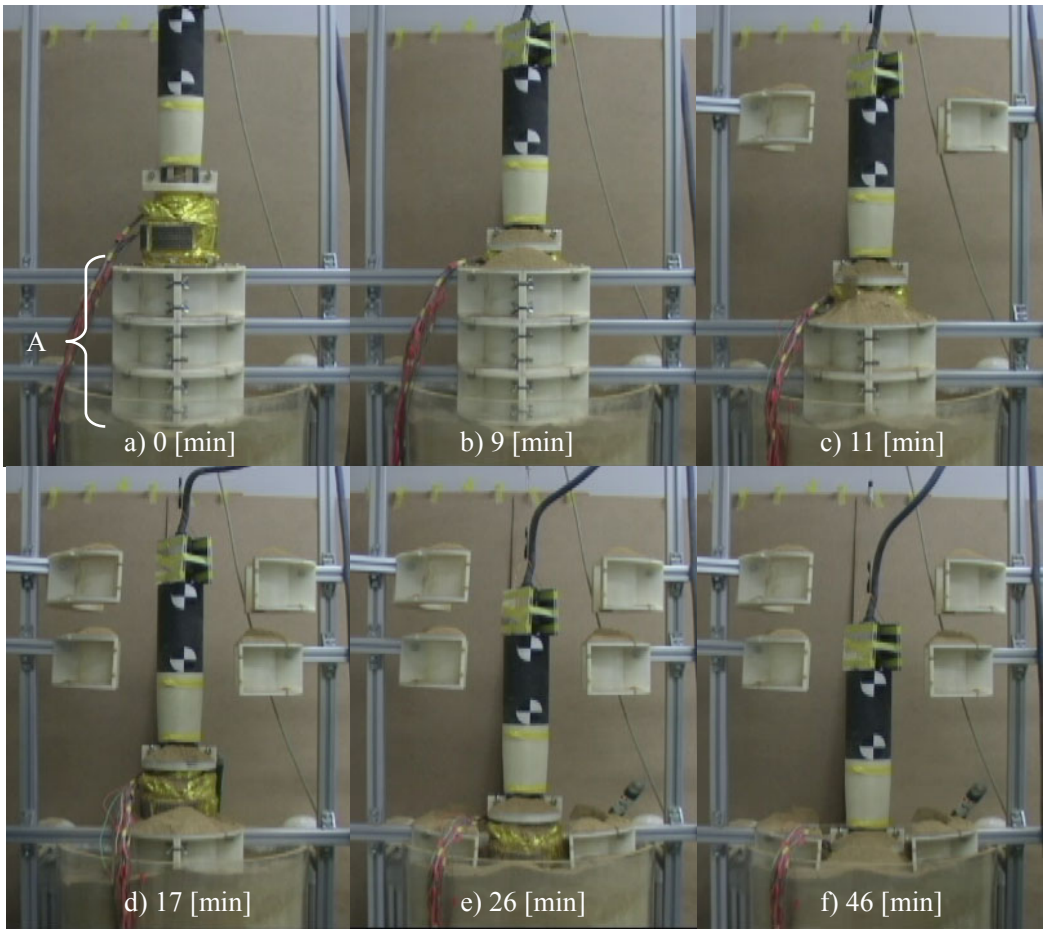


Fig. 7.7 Excavation experiments with launcher (A: Launcher)

The maximum torque was kept to less than 10 Nm, which was about 40% less than that of the excavating unit alone and favorable for overall robot motion. Except for a few seconds at this relatively large motor torque, throughout about 1-h experiment, motor torque could be further reduced by more than 70% (see Fig. 7.8).

Fig. 7.9 shows the experimental results, in terms of depth with respect to elapsed time, for the four excavation conditions used in the experiment. The average velocity of excavation was 0.19 mm/s at 52 N, 0.19 mm/s at 26 N, 0.23 mm/s at 13 N and 0.21 mm/s at 8.7 N. The average velocities for cases in which the experimental mass was 1/4 and 1/6 of the robot's weight were similar to the target velocity of 0.25 mm/s. But the velocities at 1/2 and 1/1 of the robot's weight were lower. It is believed this occurred because discharged soil fell into the excavated hole and prevented the propulsion unit from working properly. However, the excavator could bore to a depth of around 430 mm, and was expected to be able to excavate deeper because the excavation velocity did not decline except when progressing under its own full weight. Slippage was also observed as the motor torque increased, but the average motor torque was reduced to less than 5 Nm.

Through experiments, it was confirmed that the excavator was able to excavate and move at 1/6 of its own weight. Excavation deeper than 430 mm is possible by improving the discharge part of the unit. Therefore, it was concluded that the propulsion unit can maintain its body position and rotation for the most part, therefore reducing the effect of the pressure of the surrounding earth in terms of controlling "wall holding" during downwards movement.

Both the developed propulsion and excavation units proved effective for use in the prototype excavation robot.

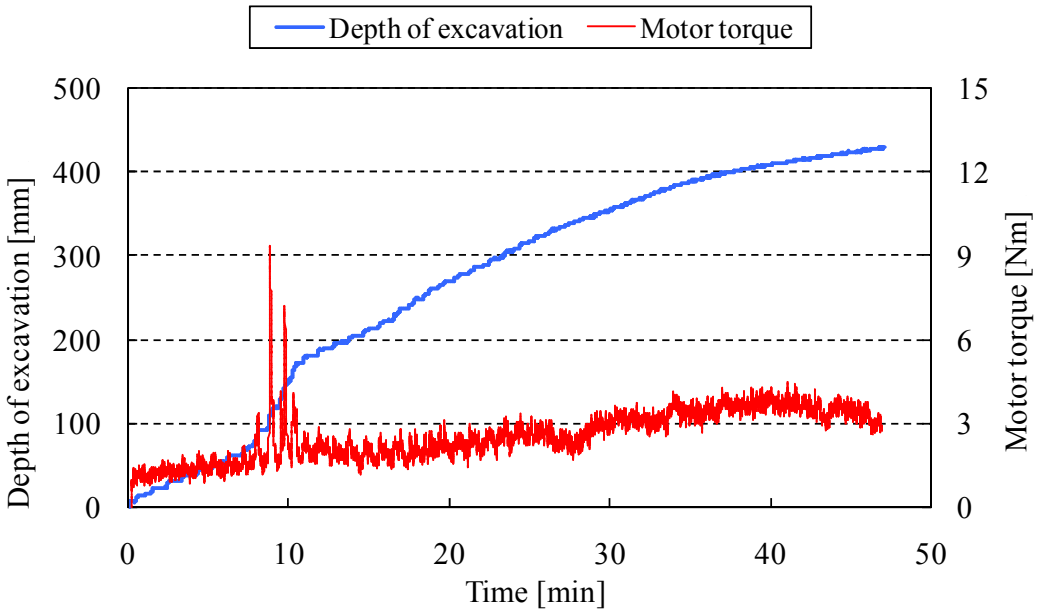


Fig. 7.8 Results of excavation (52 N)

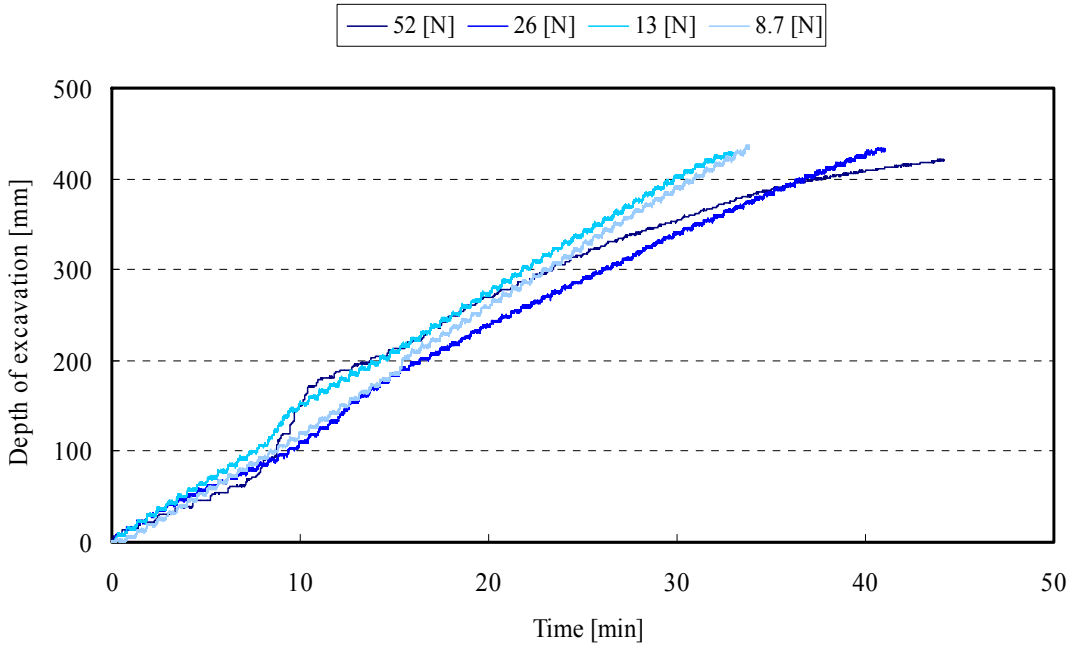


Fig. 7.9 Experimental results of different weights of the excavator

## 7.6 Experiments with Dirt Collector

As presented in previous section, the robot was able to excavate to a depth of 430 mm, then it had to stop excavating because the discharge ports reached soil level. Then, it seemed impossible to discharge further the excavated soil.

Here the excavation experiments are reported after the depth of the discharge ports reached soil level, now getting rid of the excavated soil using a dirt collector. Fig. 7.10 shows the tracks of measured excavation depth and motor torque. The robot moved inside the launcher for the first 9 min, at an average velocity of 0.23 mm/s. Then it "slipped" from 9 to 13 minutes, in a transition phase, while the launcher was being released. Then it constantly excavated from 13 minutes to the end of experiments. Here the average velocity was 0.16 mm/s. It could excavate to a depth of 650 mm until a hose pipe was unable to reach it (Fig. 7.11). In this experiment, the dirt collector removed the soil from the discharge ports. The robot could excavate to a depth of 650 mm, the tracks of excavation were constant and the velocity did not get slower. It is believed that it could easily excavate deeper than 650 mm, if the discharging process were improved. The proposed propulsion unit has demonstrated that it decreases the effect of the friction force traditionally limiting excavator locomotion. Therefore it is confirmed that the bio-inspired propulsion unit relying on peristaltic crawling and the principle of a tapering EA work effectively for an excavation robot.

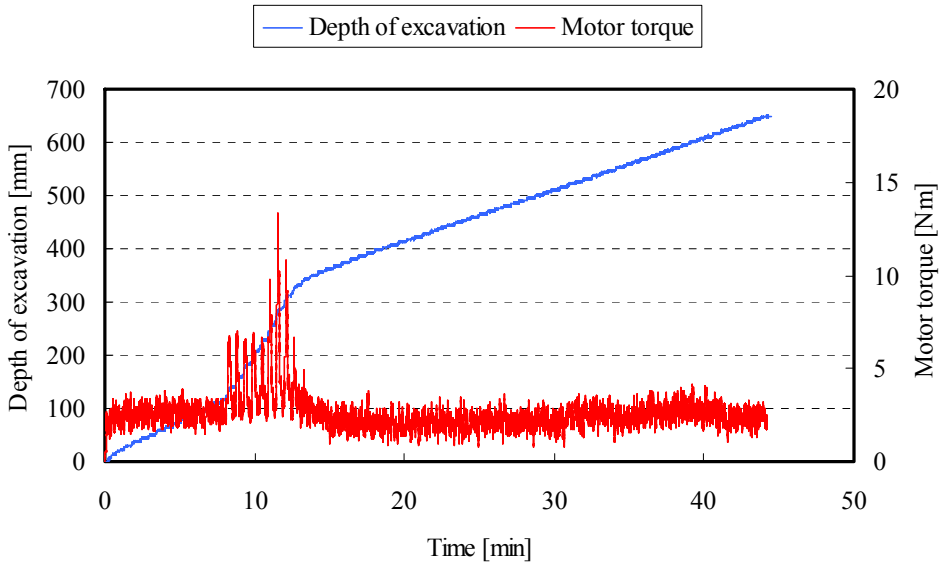


Fig. 7.10 Results of excavation with the dirt collector

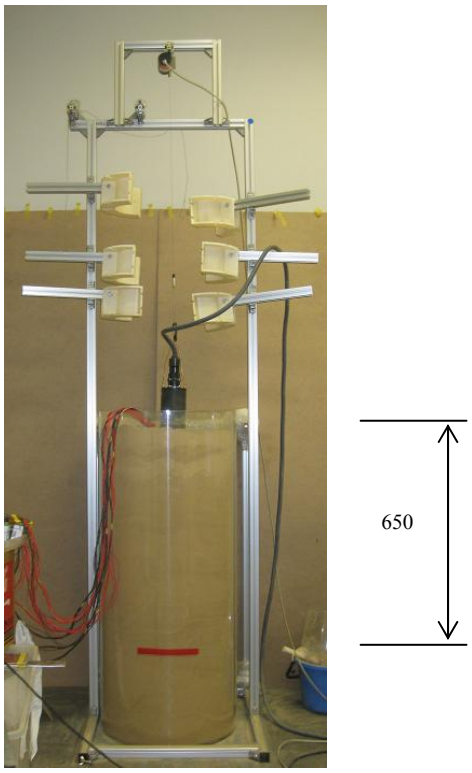


Fig. 7.11 Robot excavating a depth of 650 mm

# Chapter 8: Development of a Discharging Part

Subsurface explorer robot with propulsion and excavation units showed it could excavate deeper than the excavation unit alone, and excavate at the same depth with no reference to the weight of the robot. Nevertheless, it was not equipped with a discharging part, which hindered deeper excavation when the discharge ports of the robot reached the surface of the ground. Therefore, this section explains the development of a discharging part that can transport discharged soil from the ports to the ground.

## 8.1 Development of a Prototype Discharging Part

Fig. 8.1 images the motion of discharging part. It consists of the winder, bucket and base part. Soil discharged from the ports is collected in a mobile bucket that can be rewound by the winder. The rewound bucket above ejects the soil away from the excavated hole. Wires connect the bucket to the base part that is fixed to the robot. The base part has two flat spiral springs inside that pull the bucket downward. The empty bucket returns on the base part by controlling the winder. Fig. 8.2 shows the developed discharging part; (a), (b), and (c) of the figure are the bucket, the base part, and the internal structure of the base part, respectively. Table 8.1 lists the specifications of the discharging part. The conveyable amount of soil is calculated from the volume of the bucket and the measured soil density (0.91 g/cm$^3$). The reasons for adopting the flat spiral spring are low-gravity use, simple mechanism and easily adding sealing mechanism. The flat spiral spring within the base part meets the following criteria:

1) The pulling force of the flat spiral spring is less than the maximum traction (500 N) of the winder.
2) The pulling force is larger than the friction force generated between the robot and bucket (1.5 N) when the bucket is hoisted.

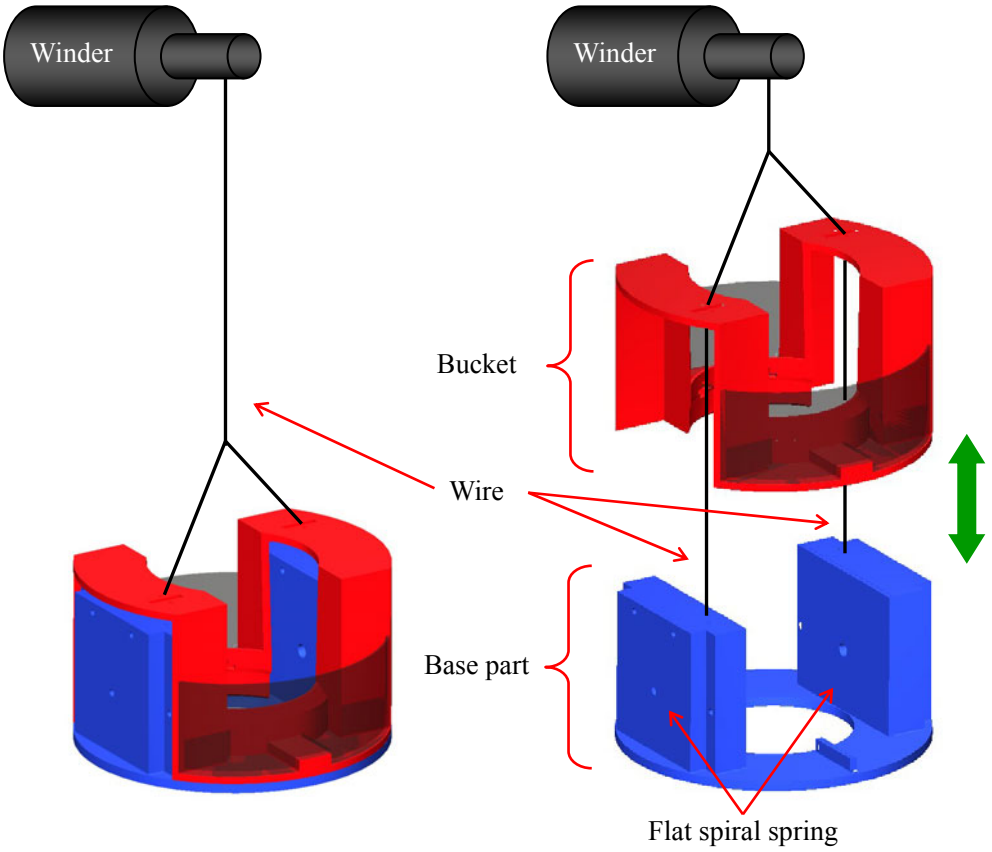


a) While discharging soil b) Winding the bucket

Fig. 8.1 Motion of discharging part


a) Bucket b) Base part c) Inside base part

Fig. 8.2 Developed discharging part

Table 8.1 Specification of the discharging part

| | | |
|---|---|---|
| Outer diameter of the bucket [mm] | | 126 |
| Conveyable volume of the bucket ($x10^3$) [$mm^3$] | | 61 |
| Conveyable amount of the soil [g] | | 55.5 |
| Weight of the discharging unit [g] | | 245 |
| Force of the flat spiral spring [N] | Max. | 3.7 |
| | Min. | 2.9 |
| Conveyable distance of the bucket [m] | | 1.5 |

## 8.2 Discharging Experiments

Fig. 8.3 shows the robot used in this experiment, comprising the excavation and discharging units; the propulsion unit is absent. The function of the discharging part is tested in the launcher and in the excavated soil by manual propulsion. In addition, the amount of discharged soil and the amount of soil dropped from the bucket were measured to evaluate this prototype discharging part. The collection part in figure collects the dropped soil. The experimental processes are listed below.

1) Robot excavates a hole by rotating its earth auger.
2) Rotation of the earth auger is manually stopped when the bucket is full of soil, assessed by a visual check.
3) Bucket is hoisted by the winder. Hoisting is halted at a certain point after the bucket has passed through the robot.
4) Soil is manually collected in the bucket.
5) Bucket is returned by control of the winder.

These processes 1–5 are repeated.

In both launcher and soil measurements, the measured excavation range is about 200 mm. The

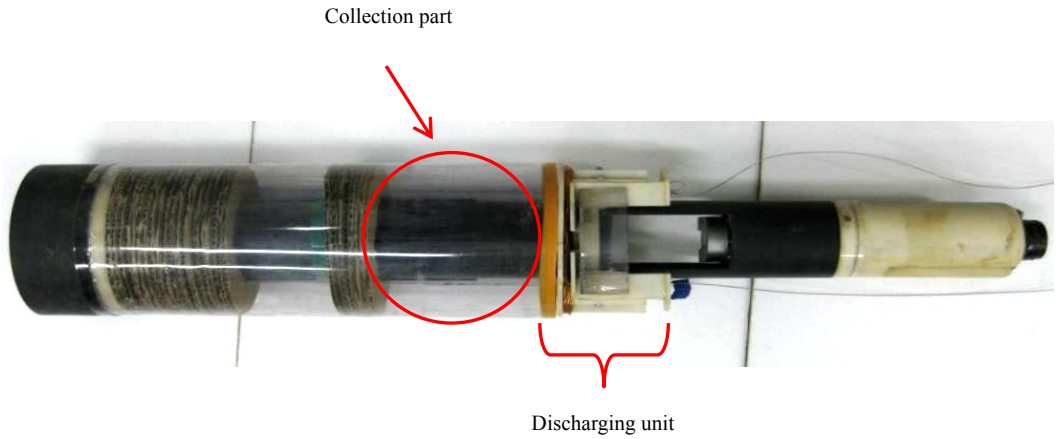


Fig. 8.3 Excavation and discharging units with the collecting part

respective excavation depths are 270–470 mm and 470–670 mm.

Fig. 8.4 shows the hoisting mechanism of the bucket inside the launcher and the soil. The bucket could be hoisted continuously against the robot, and rarely halted inside the launcher. Inside the soil, it was confirmed that the sidewall surface of the bore hole was not lopped off by the hoisting of the bucket. In the range of a 200 mm, the winching number was 41 and 45 times inside the launcher and the soil. The rates of dropping with respect to the total discharged soil from the spout were 26 and 27%.

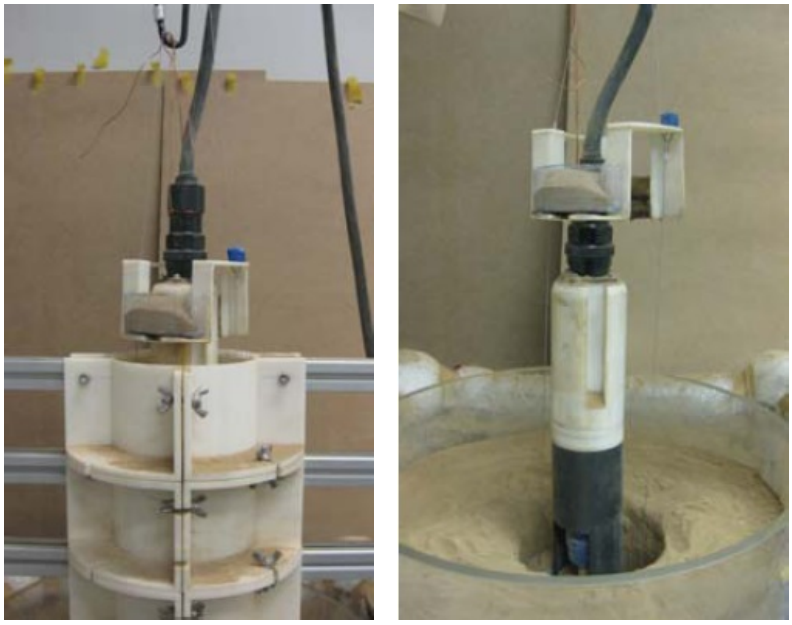

a) Inside launcher a) Inside soil

Fig. 8.4 Winching of the bucket and measure the transported soil

## 8.3 Discharging Experiment with an Excavation Robot

Finally, the discharging part was fitted to an excavation robot with both excavation and propulsion units, as shown in Fig. 8.5. The experimental setup was essentially the same as previously, with the exception of the propulsion unit. The propulsion unit was halted during bucket hoisting. In this experiment, the robot successfully excavated to a depth of 595 mm (Fig. 8.6). When the discharging unit is in the soil, the underneath of its spout is below the surface. Thus, it was confirmed that the discharging unit could carry the discharged soil when combined with an excavation robot. However, the experiment was terminated at depth 595 mm because of problems with the propulsion unit, probably caused by soil falling from the base part. Thus, it is expected that if the amount of dropped soil was decreased, deeper excavation should be possible.

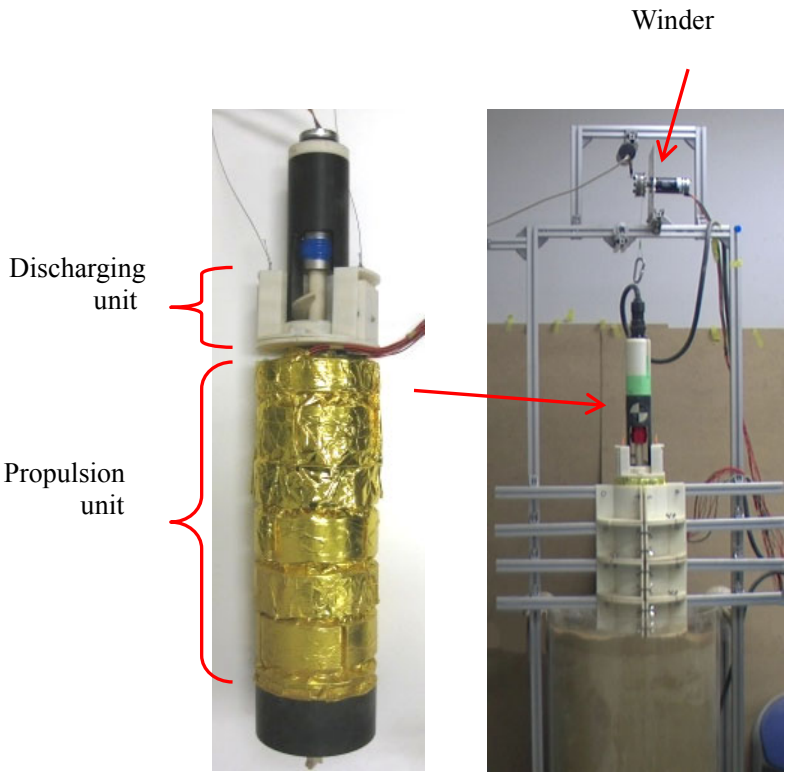


Fig. 8.5 Excavation experiments with excavation and propulsion units

Fig. 8.6 Excavation experimental results (595 mm)

## 8.4 Discussion of the Results

It was observed that over 25% discharged soil from the discharging ports was dropped from the bucket to the base part. It was considered because of the soil that covers between the EA and the bucket. Fig. 8.7 shows the cause of dropping soil. The left photo shows the condition from the experiments. The right illustrates the cause of the drop. The discharged soil covered over EA and the bucket then the bank on the EA and bucket dropped when the bucket was hoisted above because they were in unstable condition, and were not sustained by a plate. To solve this problem, two additional parts would be revised. For the bank on EA, a shutter part would be added to the screw part of the EA. It closes the spout when the bucket is hoisted. For that on bucket, a flexible fin would sweep and make it flat shape.

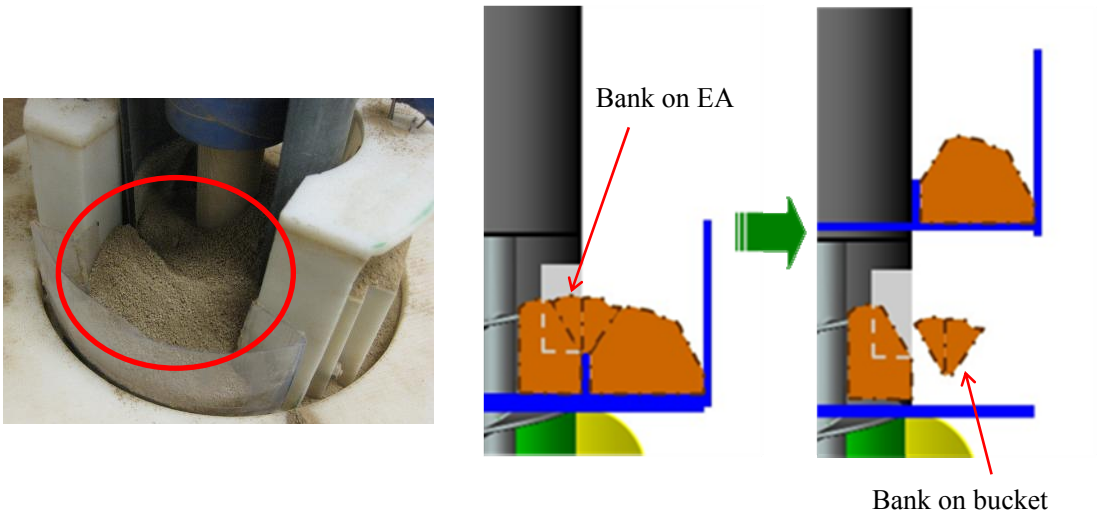


Fig. 8.7 Cause of dropping soil of the discharging part

# Chapter 9: Fundamental Experiments for Modeling the Cutting Resistance

This section explains the fundamental experiments to reveal the excavation process and rate of cutting torque on the EA for modeling the excavation torque at the next step.

## 9.1 Definition of Excavation Resistance

The excavation resistance is defined as the resistance when the EA of the excavation unit excavates, transports and discharges. The modeling of this excavation has great benefits for an excavation robot as demonstrated in Fig 9.1. Excavation resistance is calculated taking conditions and environment such as material, depth, density, rotation speed, and pushing force into consideration. If it is modeled, it would realize efficient excavation of EA, to reveal requirements for a propulsion unit, and efficient excavation propulsion. However, the model would be complex because of including many parameters as mentioned before, so the maximum excavation torque will first calculate. This also offers an important benefit since requirements of a maximum motor torque of an excavation unit then it will be downsized.

This resistance is classified into cutting resistance, transport (Fig. 9.2) and discharge. The cutting resistance works at the head of the EA composed of a fish tail and a screw part with bits, ahead of the excavation support. The transport resistance works in the process of transporting soil with a screw part of EA inside the excavation support. Table 9.1 shows the effect of different conditions, materials, and the

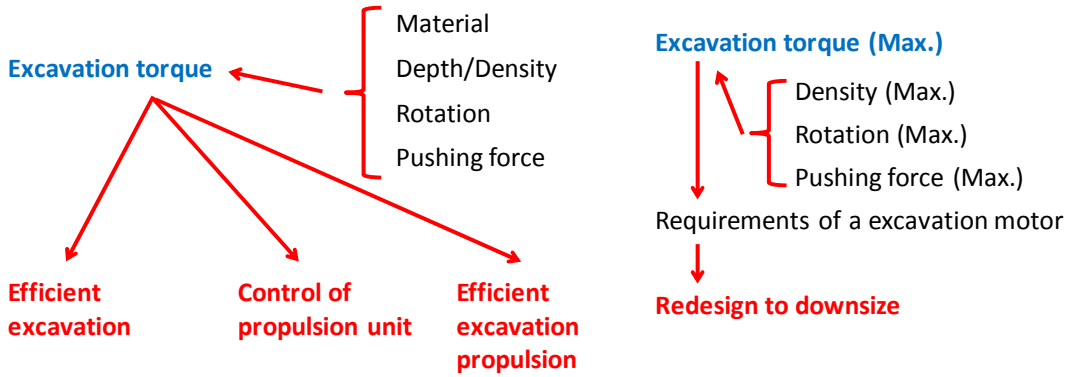


a) Total benefits b) First aim

Fig. 9.1 Benefits to excavation resistance model

robot to these resistances. The pushing force and rotation speed of the EA against the front soil, are controlled by the propulsion unit. Therefore, soil types and conditions such as the density and the pushing force of the EA affects the cutting resistance. On the other hand, the excavation support covers the outside of the transport part, so the transport resistance, which is constant when it is totally filled with the excavated soil, is not affected by the depth of excavation. Moreover, the propulsion unit maintains these resistances to control the position, orientation and propulsion. The excavator can move with efficient excavation and propulsion motions if the excavation resistance is modeled and predicted.

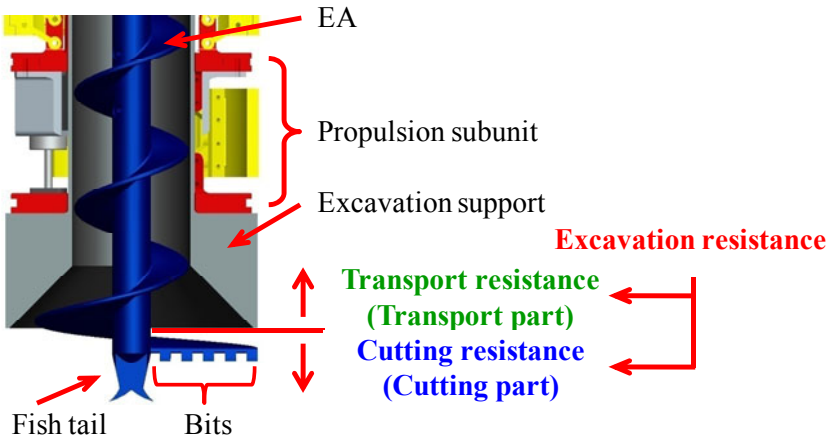


Fig. 9.2 Details of EA and the excavation unit

Table 9.1 Conditions of excavation resistance

(○: significant, △: slight, ×: none)

| | Materials | | Robot | |
|---|---|---|---|---|
| | Materials | Depth / Density | Rotation speed | Vel. / Pushing force |
| Transport resistance | ○ | × | △/× | × |
| Cutting resistance | ○ | ○ | △/× | ○ |

## 9.2 Experimental Conditions

Fig. 9.3 shows the process of excavation in 2-D. The red arrow in figure (a) presents the excavation direction. EA is rotated by a motor of excavation unit and moved down by a propulsion unit. Therefore, it moves at an angle. Here, the rotation force ($F_{Sc}$) and downward force ($P_{Sc}$) works on the screw part as illustrated by the green arrows in figure (b). The screw receives the reaction force ($F'_{Sc}$) that would be from the force ($G_{Sc}$) on a slip surface and the weight ($W_{SSc}$) of cut soil. The top of screw also receives the reaction force ($P'_{Sc}$) against the pushing force ($P_{Sc}$). In the same way, the FT receives resistant forces ($F'_{FT}$, $P'_{FT}$) against the rotation force ($F_{FT}$) and the pushing force ($P_{FT}$).

In the actual cutting process, the EA moves at an angle, which is considered to continue moving with tiny rotational and downward movements. Hence, this tiny cutting movement is taken into consideration in this chapter, so the downward movement is set before the beginning of cutting experiments. Four cutting experiments (Fig. 9.4) are carried out to reveal the excavation process as follows:

1) Pushing force experiments

As seen (a), an initial vertical force is added to the EA with the FT and cutting experiments are

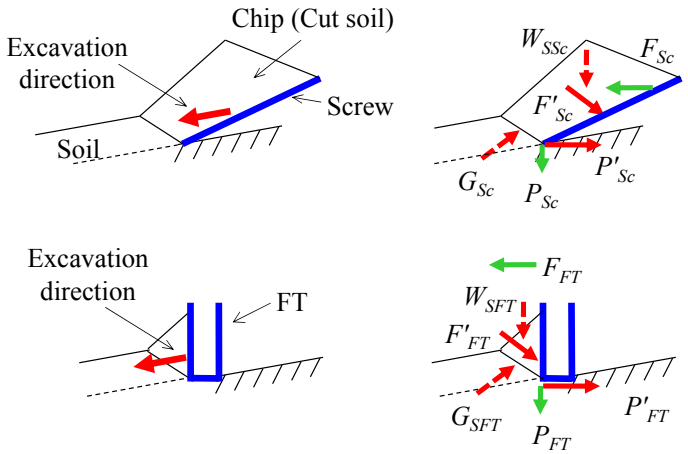


a) Cutting process b) Cutting model

Fig. 9.3 Cutting process and outline of cutting model

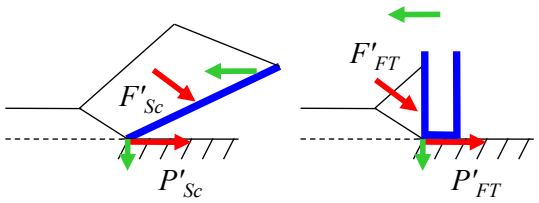


a) Pushing force and rotation speed experiments

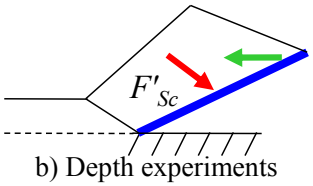


b) Depth experiments

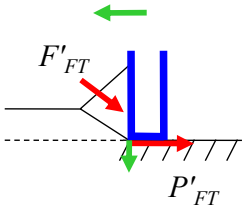


c) FT experiments

Fig. 9.4 Different patterns of experiments

conducted. Resistance forces ($F'_{Sc}$, $F'_{FT}$) against rotation and forces($P'_{Sc}$, $P'_{FT}$) against pushing force is measured.

2) Rotation experiments

The same EA as the previous experiments is used here. An initial pushing force is not changed and rotation of EA is changed, which the effect of rotation speed is measured.

3) Depth experiments

As seen (b), cutting depth is changed in this experiment. Therefore, the resistance torque is measured with respect to the force ($F'_{Sc}$).

4) FT cutting experiments

As seen (c), an initial pushing force is added, and the FT conducts cutting in these experiments. The resistance torque is measured with respect to the force ($F'_{FT}$) and pushing force($P'_{FT}$). In the end, the resistance of FT is revealed against total resistance of EA.

## 9.3 Experimental system

Fig. 9.5 shows the experimental device for soil cutting of the EA. A DC motor (EC, 45 flat 30 Watt, Maxon) is mounted on a linear stage for controlling the pushing force of the EA. This stage vertically moves with ball screw mechanisms. There is a 6 axis force sensor (LAT-1000KA-1, KYOWA) between the motor and the EA to measure the torque and vertical force. The vertical compress direction to the sensor is defined as positive. The right-hand screw direction along the positive vertical force is defined as a positive torque. The EA for in this figure has the maximum radius of 65 mm and 5 bits at the top of screw

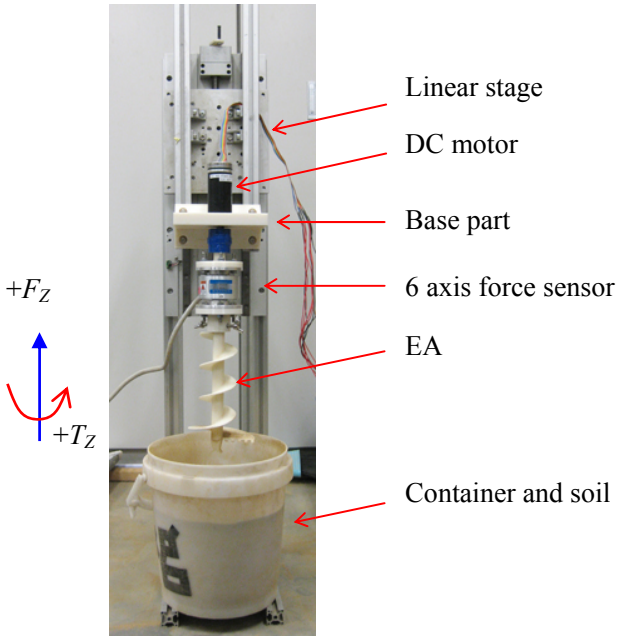


Fig. 9.5 Experimental system for cutting of EA

part. The red soil is set in the canister with a height of 270 mm and a diameter of 236 mm. The soil, which is compacted each 4 layer, fills with 130 mm high of the canister, in a density of 1.1 g/ $cm^3$. The soil is reset for every experiment to make even condition.

Fig. 9.6 shows the controlling system of cutting experiment. The motor for the EA is connected to a note computer via the motor controller (EPOS2 45/5, Maxon). The 6 axis force sensor is connected to a signal processor (FDP-106A) which digitally decreases interference against other axis and outputs an analog voltage. This voltage is received and converted to digital data by the AD board (LANM3069, TECHNO WAVE). C# program is used to control and receive the data from the motor controller and the AD board on account of features of programmer friendly with various libraries and graphical user interface.

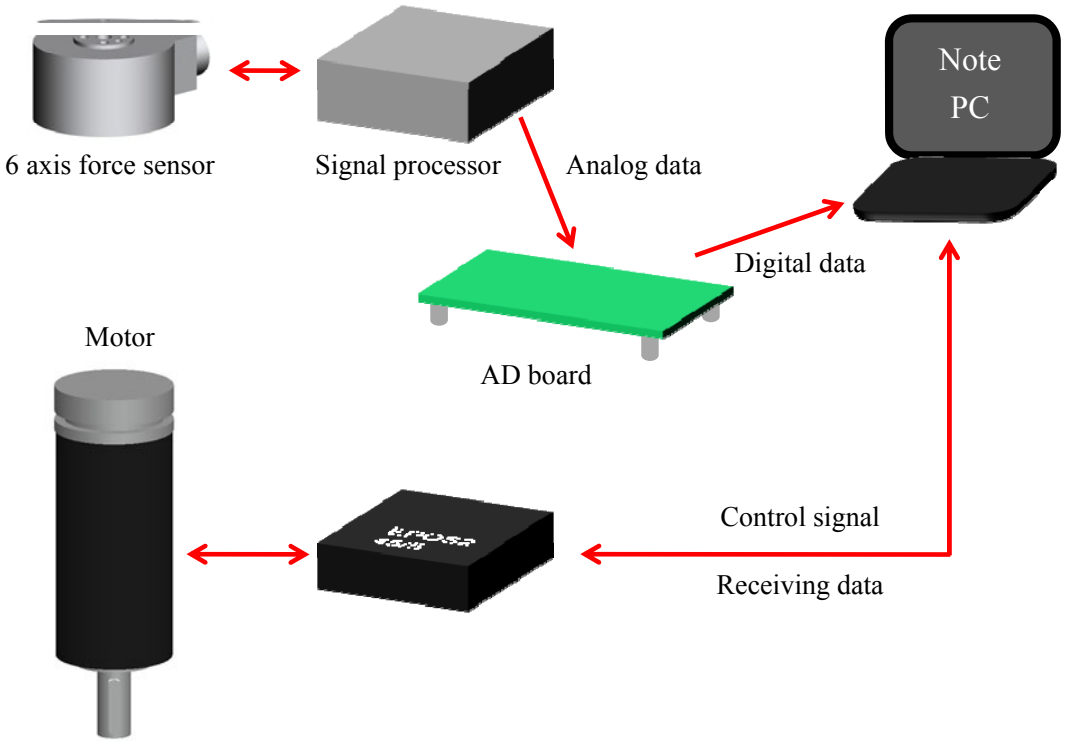


Fig. 9.6 Controlling system

## 9.4 Pushing and Rotation Experiments with EA

This section focuses on the cutting resistance to reveal the excavation process by the experiments. In the cutting process, a fish tail and the screw with bits cut the front soil. Two experiments were conducted: pushing and rotation experiments.

### 9.4.1 Conditions for Pushing and Rotation Experiments

Table 9.2 lists the details of the pushing and rotation experimental conditions. In the pushing force experiments, first the stage moves downward and the EA is pushed to the soil with monitoring the vertical force from the 6 axis force sensor. When the force reaches 60, 160 and 260 N, the position of the stage is fixed and the EA rotates at 10 rpm and 360 degrees. In the rotation speed experiments, the EA is set at a pushing force of 160 N the same way as the pushing force experiments. Then it rotates at 3, 5, 10 rpm, respectively. The detail conditions of the experiments are shown in Table 9.2, which illustrates that soil conditions are nearly the same in each experiment.

Table 9.2 Pushing and rotation experimental conditions

| Name | Rotation speed | Acceleration | Rotation | Pushing force |
|---|---|---|---|---|
| | [rpm] | [rpm/s] | [deg] | [N] |
| **Pushing force experiments** | | | | |
| P60 | 10 | 500 | 360 | 60 |
| P160 | 10 | 500 | 360 | 160 |
| P260 | 10 | 500 | 360 | 260 |
| **Rotation speed experiments** | | | | |
| R3 | 3 | 500 | 360 | 160 |
| R5 | 5 | 500 | 360 | 160 |
| R10 | 10 | 500 | 360 | 160 |

### 9.4.2 Pushing Force Experiments

Fig. 9.7 shows the EA excavating the soil at a pushing force of 160 N. (i) shows the EA set just above the soil, (ii) its pushing force reached to 160 N just before starting the rotation, (iii) it rotated 240 degrees and (iv) it reached 360 degrees and stopped. Fig. 9.8 shows the measured values and (a) and (b) are the vertical force and the rotation angle, and the torque and the rotation angle in the pushing forces of 60, 160 and 260 N, respectively. In (a), three patterns showed almost the same

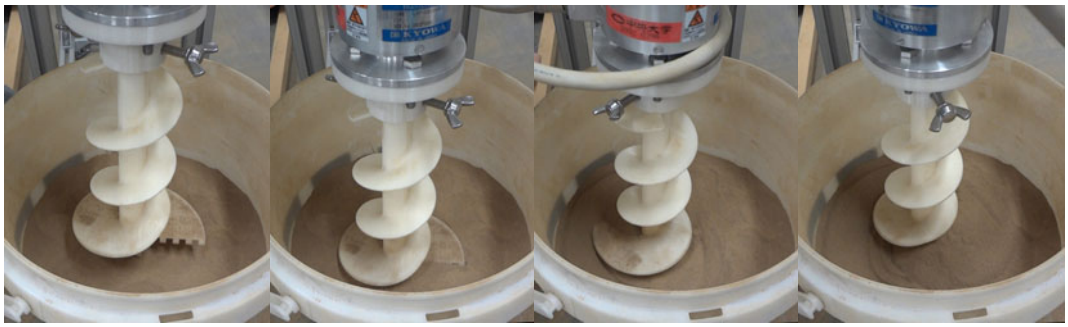

i) Before 0 [s] ii) 1 [s] iii) 5 [s] iv) 6 [s]

Fig. 9.7 Example of the experimental results (160 [N], 10 [rpm])

tendency. The vertical forces gradually decreased after starting the rotation and slightly increased from around 4 s. The three patterns of torques in figure (b) also showed a similar tendency. The peak motor torques were observed at the beginning of the rotation. The torques decreased soon after the

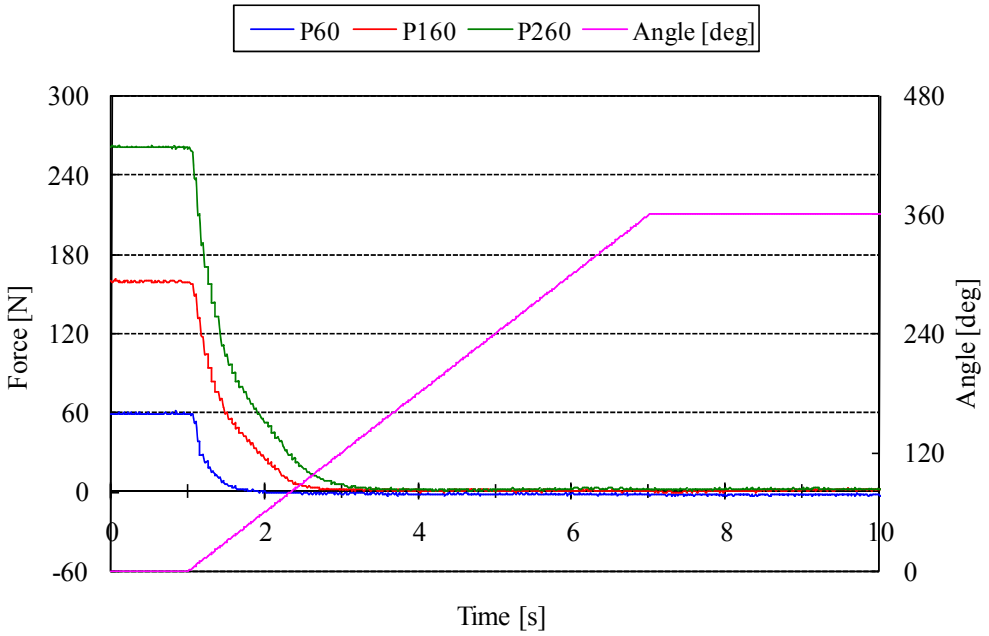


a) Vertical force

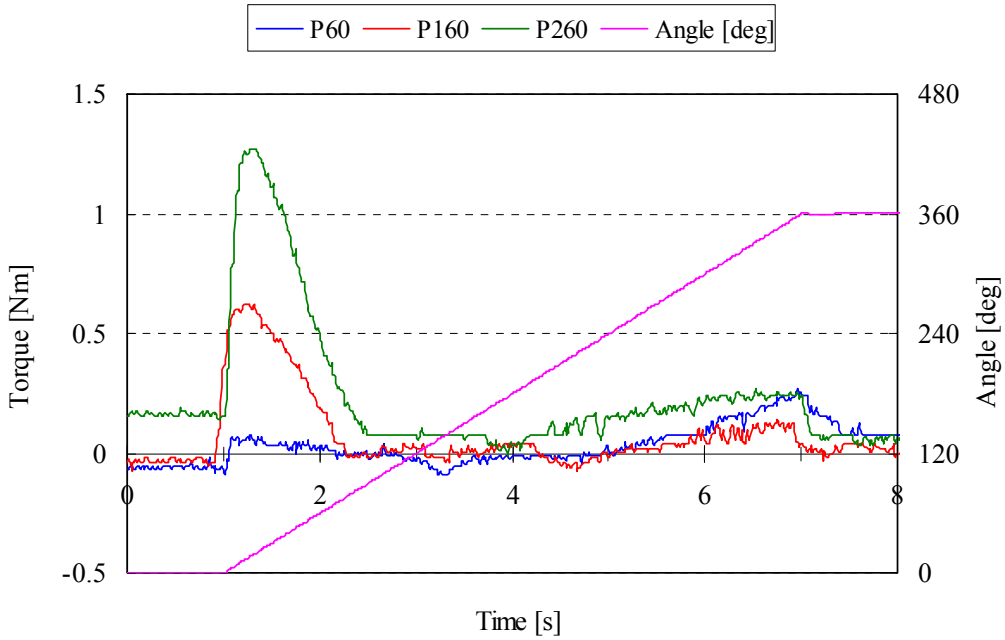


b) Torque

Fig. 9.8 Comparison of pushing force experiments
(Pushing force 60, 160, 260 [N], rotation speed 10 [rpm])

peaks then gradually increased after around 4 s. The second peaks of torques were observed at the end of the rotation. The maximum torques in relation to the pushing force were observed at the beginning of the rotation when the pushing force was large e.g., 160 and 260 N but it occurred in the end of the rotation when the force is small e.g., 60 N. The peak torques throughout experiments are listed in Table 9.3. The first peak was observed at the beginning of experiments. On the other hand, second was at the end of experiments. Settlement of EA were 4.8 mm at P60, 9 mm at P160 and 12.1 mm at P260. These values are used to compare with the depth experiments of a screw part.

Table 9.3 Peak torques in pushing experiment [Nm]

| | 1st Peak | 2nd Peak |
|---|---|---|
| P60 | 0.072 | 0.273 |
| P160 | 0.623 | 0.141 |
| P260 | 1.26 | 0.255 |

**9.4.3 Rotation Speed Experiments**

Fig. 9.9 shows the experimental results of rotation speed. (a) and (b) show the vertical force and the torque, respectively. Vertical lines in the figures describe the end of the rotation. The dashed line, dashed-dotted and dashed-two dotted correspond to R3, R5, R10 respectively. In (a), the force of three different rotation speeds decreased from the beginning of the rotation the same as the results of the pushing force experiments. The forces just before the end of rotation were 0.9 N at R3, 0.9 N at R5 and 0.5 N at R10. In (b), three patterns showed a similar tendency. Table 9.4 lists the peak torques. The tracks were seen to be scale-up and down along the time. The peaks and maximum of torques were observed at the beginning of the rotation. The torque became slightly smaller when the rotation speed was faster.

Table 9.4 Peak torques in rotation speed experiment [Nm]

| | 1st Peak | 2nd Peak |
|---|---|---|
| P3 | 0.745 | 0.165 |
| R5 | 0.667 | 0.188 |
| R10 | 0.623 | 0.078 |

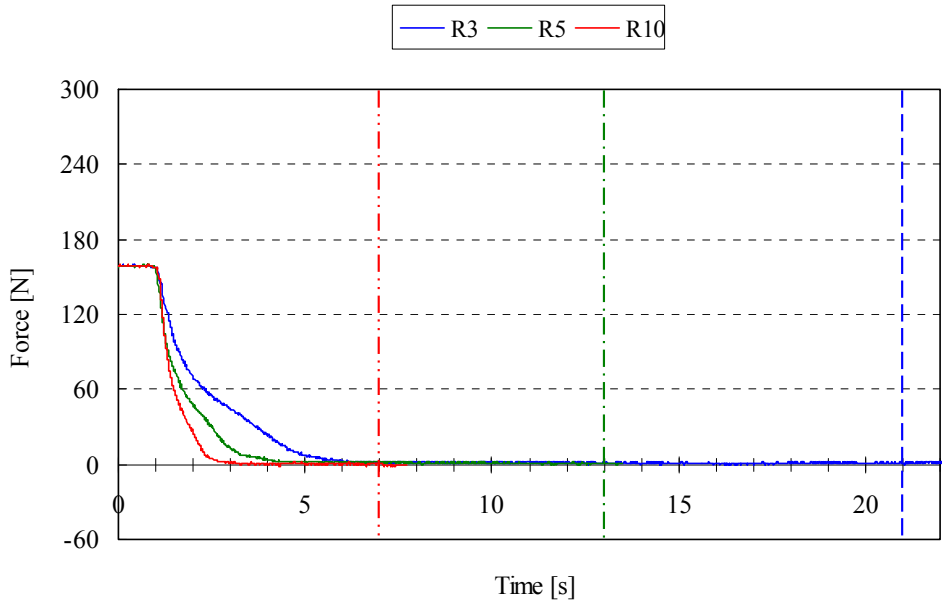


a) Vertical force

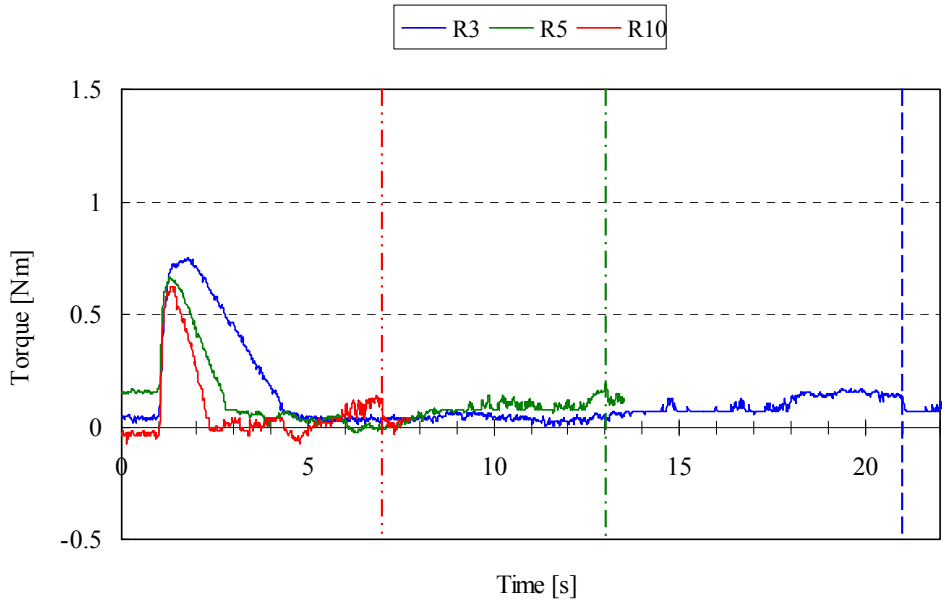


b) Torque

Fig. 9.9 Comparison of pushing force experiments
(Pushing force 160 [N], rotation speed 3, 5, 10 [rpm])

### 9.4.4 Discussion of Soil Cutting Experiments

According to the pushing force experiments, it is considered that the drop of the force in the beginning of the rotation was due to the three different pushing forces, which were added before the

beginning of the rotation, were not added after the rotation. At the time, the torque increased then decreased. It was considered it was due to the friction between the back surface of the EA and the soil because the vertical force was also large. From in the middle of the rotation, the torque gradually increased. It was considered the cause of cutting resistance and the resistance to push away the cut soil in a radial direction. To calculate the required torque, soil cutting model with respect to the pushing force, soil cutting and force of pushing away material would be needed.

According to the rotation speed experiments, it was found that the torque does not significantly change when the rotation speed becomes faster. Therefore, it can be considered that the tendencies are the almost same in different rotation speeds. On the other hand, the force and torque show slightly different values when the pushing force differs. However, we could assume that they are almost equal values.

## 9.5 Depth Experiments with Screw Part

In this section, cutting depth was changed with a screw part of EA that was not equipped with a fish tail as illustrated in Fig. 9.10. The initial pushing force was not added and the depth ($d_C$) were 5 and 10 mm with taken the results of pushing force experiments (9.4.2). The soil under the screw was removed in order to set it with nearly zero pushing force. In case of deeper than 10 mm, large area of soil is needed to remove since the angle of screw part is narrow. For this setting, experiment deeper than 10 mm was not conducted. The cutting resistance ($F'_{Sc}$) is measured in Fig. 9.10.

Fig. 9.11 shows the cutting experiments results. (a) and (b) demonstrate the vertical force and torque, respectively. From (a), both D5 and D10 pulled vertical downward direction, and the minimum values were -2.1 N and -1.1 N. From (b), torque of both condition increased slightly and the maximum values were 0.09 N (D5) and 0.16 N (D10). Table 9.5 summarises the maximum torque compared with the pushing force experiments. Depth between the pushing force and depth experiments were a little different but they are compared as a references value. It was found that the cutting resistance of screw part account for 34% and 26% of the total resistance.

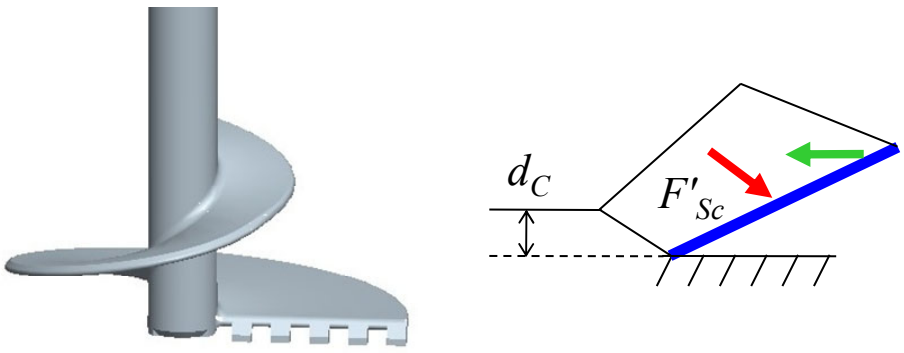


Fig. 9.10 EA without FT

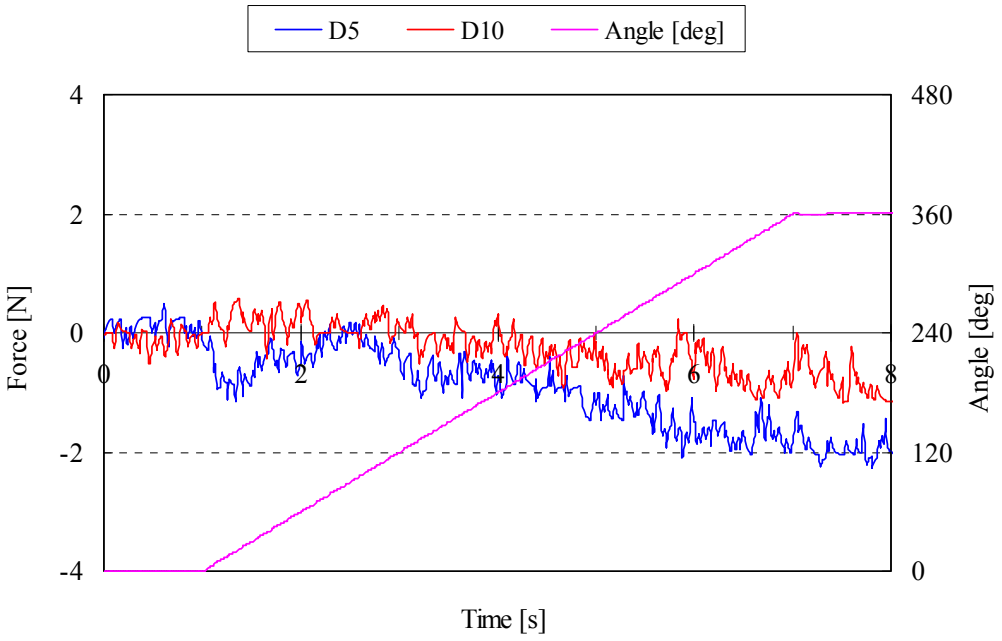


a) Vertical force

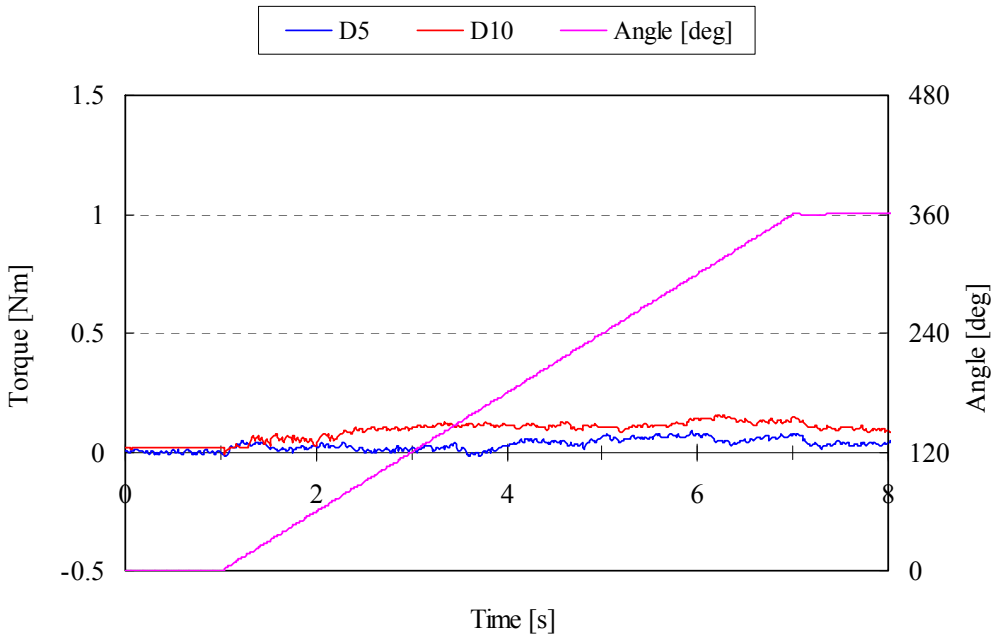


b) Torque

Fig. 9.11 Comparison of depth experiments with screw of EA
(Depth 5, 10 [mm], rotation speed 10 [rpm])

Table 9.5 Results and comparisons between pushing force and depth experiments

| EA | | Screw | | |
|---|---|---|---|---|
| Experiments | Max. torque | Depth | Max. torque | Percentage |
| | [Nm] | [mm] | [Nm] | [%] |
| P60 | 0.27 | 5 | 0.09 | 33 |
| P160 | 0.62 | 10 | 0.16 | 26 |
| P260 | 1.26 | | | |

## 9.6 Soil Cutting Experiments with the Fish Tail

The soil cutting experiments with the EA were conducted in the previous section. Here, the effect of the fish tail at the head of EA is examined. First, to examine a rate of the pushing force on the fish tail, an EA with a pushing force sensor in-between the shaft is developed. From this result, experiments are conducted with the fish tail drill to measure the torque.

### 9.6.1 Measurement of Pushing Force Distribution

Here, a rate of the pushing force on the fish tail was examined. Fig. 9.12 shows the developed EA with the pushing force sensor (FlexiForce A201-100, Nitta). The EA was pushed to the soil with monitoring the vertical force from the 6 axis force sensor. The value of the pushing force sensor was measured when the target forces reached 60, 160 and 260 N. Each value of the pushing force sensor was measured three times. Fig. 9.13 shows the results. The horizontal axis and vertical axis describe the target forces of the 6 axis sensor and the rate of force worked on the fish tail, respectively. The

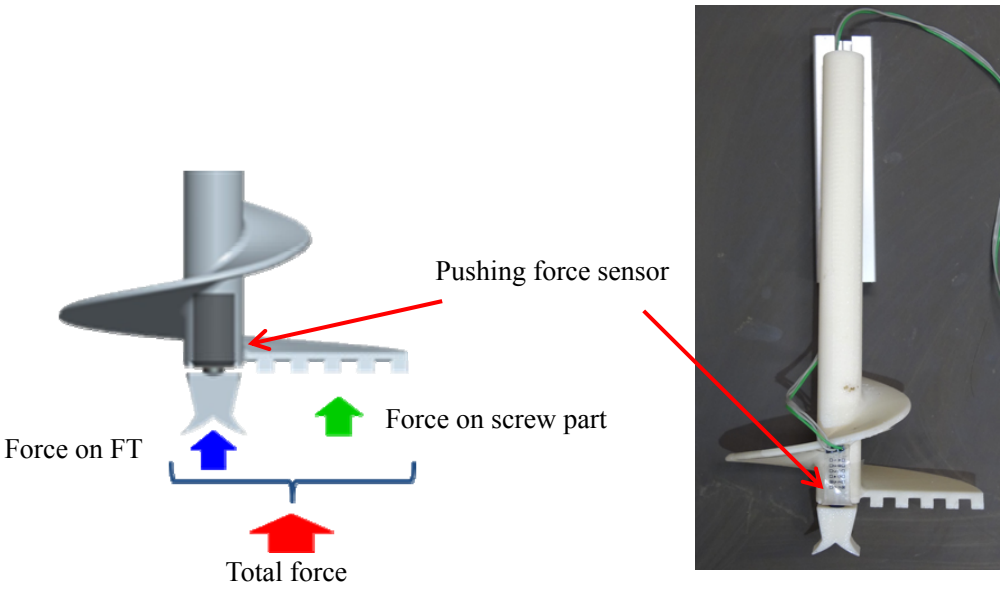


Fig. 9.12 EA with a pushing force sensor

rates were calculated by the force on the fish tail divided by the target force. The error bars describe the maximum value and minimum. In this figure, the force on the fish tail, accounted for around 60%, at 60 N. It describes that the fish tail sustains the pushing force of 60% out of the total and screw part and bits sustain that of 40%. Then it gradually decreased and accounted for around 40% at 260 N. The average pushing forces on the fish tail were 34.5, 66.0 and 93.5 N, respectively.

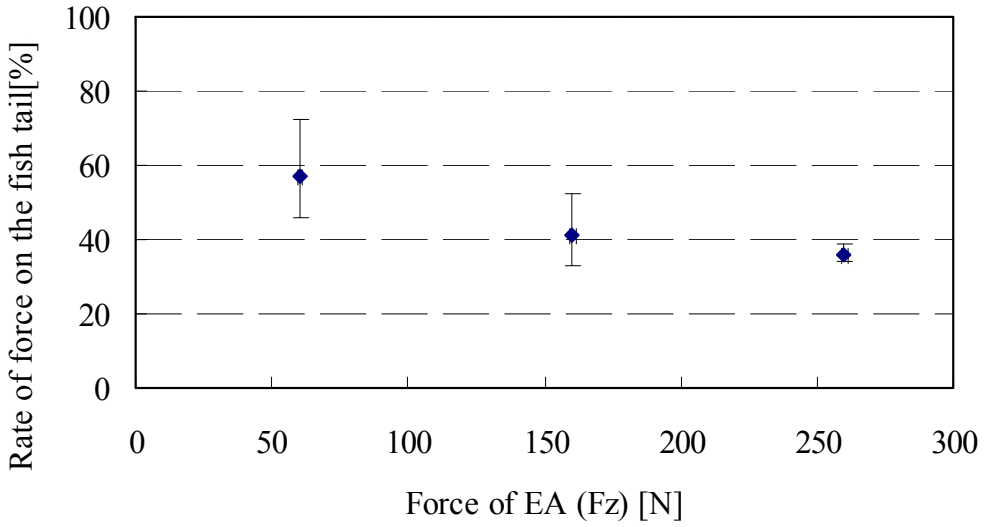


Fig. 9.13 Results of pushing force experiments

### 9.6.2 Measurement of Torque of the Fish Tail

Next, the torque of the fish tail was measured using the pushing forces measured in the previous experiments. The fish tail drill was used in this experiment (Fig. 9.14). The pushing forces of 34, 66 and 93 N were applied and the torque was measured. Fig. 9.15 (a) and (b) show the results of the vertical force and the torque, respectively. Figure (a) shows the similar results to the soil cutting experiments of the EA. In (b), the torque of three patterns vibrate through a rotation but the total value became larger when the pushing force increased. The maximum values were 0.10 N at P34, 0.13 N at P66 and 0.19 N at P93. Table 9.6 shows the occupied rate of the maximum torque of the fish tail against the EA. The rate of the fish tail against the EA was calculated by the division of the maximum torque of the fish tail by that of the EA. The torque of the fish tail occupied 15% therefore the torque of the fish tail is not negligible. The effect of the fish tail needs to be considered for the soil cutting process.


Fig. 9.14 Fish tail drill

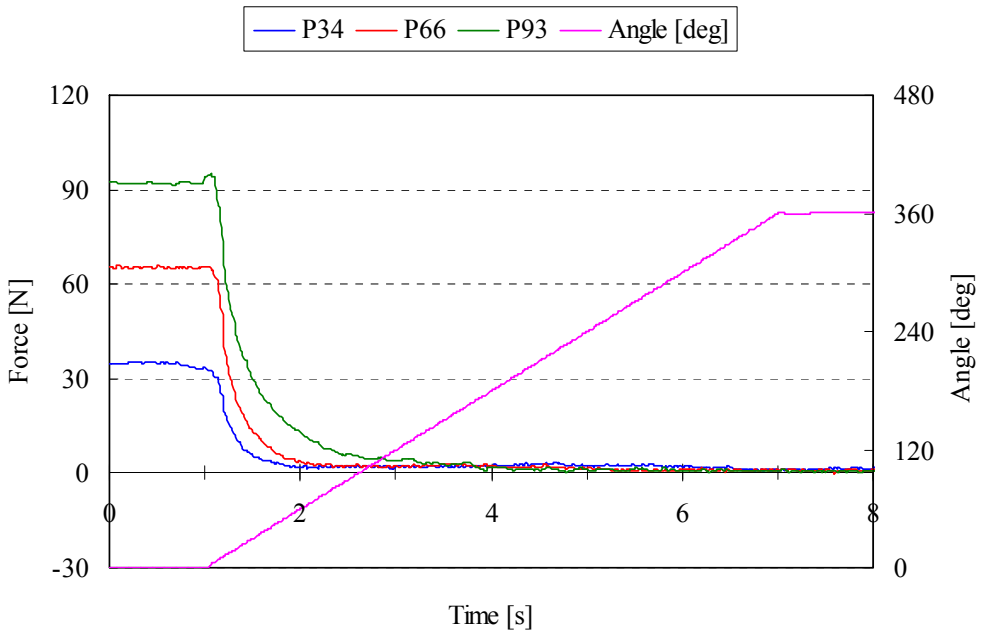


a) Vertical force

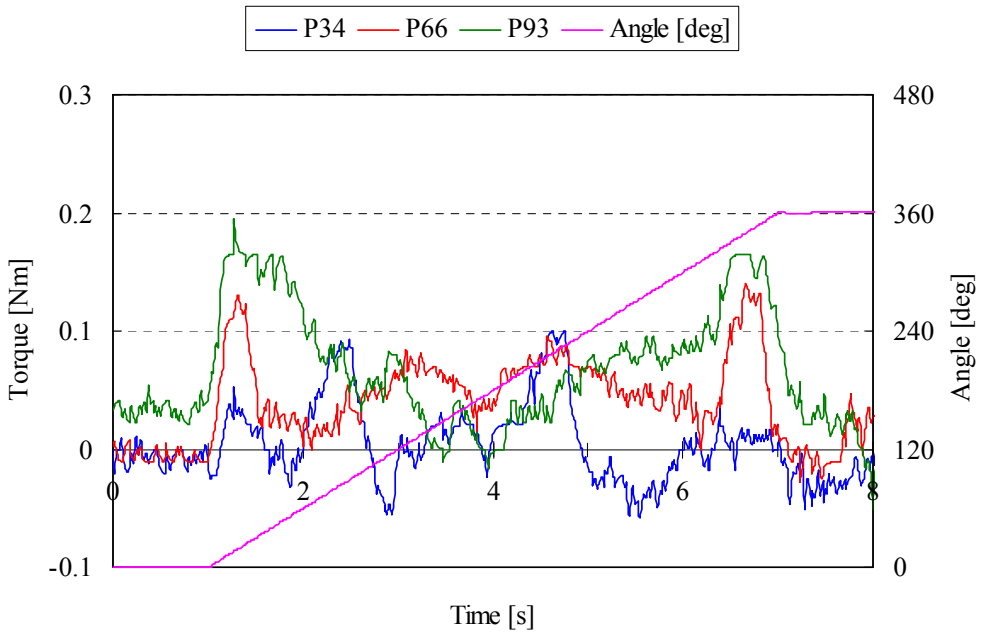


b) Torque

Fig. 9.15 Comparison of different pushing force of the fish tail
(Depth 5, 10 [mm], rotation speed 10 [rpm])

Table 9.6 Torque of the FT against the EA

| EA | | Fish tail | | |
|---|---|---|---|---|
| Experiments | Max. torque [Nm] | Experiments | Max. torque [Nm] | Percentage [%] |
| P60 | 0.27 | P34 | 0.10 | 37 |
| P160 | 0.62 | P66 | 0.13 | 21 |
| P260 | 1.26 | P93 | 0.19 | 15 |

# 9.7 Evaluation of Excavation with Mechanical Specific Energy

From, Chapter 9.4, it was found that the excavation torque greatly increases when the pushing force increases but it rarely increases when the rotation speed is faster. Here, the results of pushing force experiments are evaluated by using mechanical specific energy (MSE) proposed by Pessier et al. [86]. This MSE is widely used to evaluate the drilling efficiency for various environments [87]–[91] such as drilling soil, rock and regolith, on the Earth, or in the seabed. MSE represents the total energy (pushing force and drilling torque) with respect to excavated volume. Its equation is as follows [86]:

$$MSE = \left( \frac{PF}{A} + \frac{120 \times \pi \times RPM \times T}{A \times ROP} \right) \tag{9.1}$$

Here, $PF$ is pushing force, $A$ is drilling area, $RPM$ is rotation speed, $T$ is torque, $ROP$ is rate of penetration. The drilling efficiency is high, and consumes less energy when the MSE is small. The calculated results from the pushing force experiments are listed in Table 9.7. The $A$ was excavated area with a diameter of 0.13 m of the EA. The $T$ was the maximum torque from the experiments. The ROP was calculated from the settlement at the beginning of the experiments. From the results of MSE, P60 required least excavation energy among the three conditions and required about half the energy of P260 but was about 2.5 times slower. A propulsion unit can control the pushing force of

Table 9.7 Calculation of MSE

| | Pushing Force ($PF$) | Rotation Speed ($RPM$) | Torque ($T$) | Rate of Penetration ($ROP$) | **Mechanical Specific Energy (*MSE*)** |
|---|---|---|---|---|---|
| | N | prm | Nm | m/hr | **kJ/m$^3$** |
| **P60** | 60 | 10 | 0.27 | 2.9 | **31.1** |
| **P160** | 160 | 10 | 0.62 | 5.4 | **44.7** |
| **P260** | 260 | 10 | 1.26 | 7.3 | **68.9** |

EA to the soil. Therefore, excavation condition of the robot can be controlled with full use of the both propulsion and excavation units such as fast excavation with large energy consumption and slow excavation with small energy consumption. The feature of controlling energy consumption is useful for aerospace use, where the energy consumption is a more important factor than the speed.

# Chapter 10: Conclusion

## 10.1 Summary of Dissertation

This section summarises the paper following each chapter.

**Chapter 2: Related Research**

This chapter first introduced some heavy machinery used on the Earth for excavation but they tend to be large in size. Then three conventional types of excavator for the Moon and planets were explained. It was concluded that the subsurface explorer type is suitable for aerospace explorer mission with the remarkable features such as small, reusable. Next, thirteen designed or developed small subsurface explorers were introduced and discussed by their performances of excavation regarding the diameter vs. reached depth, and mechanisms regarding making a space and advancing forward. It was revealed that it is difficult to excavate deep when its diameter becomes larger because of the earth pressure that prevents from excavating and difficulty in making a large space for propulsion. The effect of the earth pressure to the propulsion inside the excavated hole was introduced by using the depth prediction model. Therefore, this study focuses on an excavator with propulsion and excavation units to excavate deep by tackling the two problems.

**Chapter 3: Peristaltic Crawling of an Earthworm**

The excavation robot in this study is based on the peristaltic crawling of an earthworm for the propulsion unit. This chapter described the mechanism and motion of the peristaltic crawling. Inner muscle structure was illustrated from references. To reveal and compare its motion with a developed robot, locomotion of the peristaltic crawling is videotaped and analysed. The results show a stair shape and the contraction begins from the anterior part of the earthworm and continuously propagates toward the posterior part.

**Chapter 4: Concept of a Novel Subsurface Explorer Robot**

This chapter presented detailed concept of a novel subsurface explorer robot which has a propulsion and excavation units based on the peristaltic crawling of an earthworm and an earth auger. Different mechanism from other excavation robots was formulated. Moreover, great possibility for deep excavation was discussed with solving the traditional problems of making a space and

advancing forward. In the end, detail mission process was demonstrated with full use of mechanism, which showed the robot makes the hardware system simple due to the peristaltic crawling of the propulsion unit.

**Chapter 5: Development of an Excavation Unit**

This chapter first presented the development of tapering earth auger. The model the EA was demonstrated to calculate the tracks of the edge of EA and volume inside. Next, an excavation unit was developed and conducted experiments: pushing force and rotation speeds. The former experiment showed that the reached depth was related to the weight of the robot. It was because of the earth pressure around the surface of robot. Nevertheless, the excavation velocity slightly increased with respect to larger weight. The latter showed that the reached depth was almost the same and the required motor torque showed slight differences. The requirements were measured for the propulsion unit to maintain the orientation and position against a maximum excavation reaction.

**Chapter 6: Development of a Propulsion Unit**

This chapter first introduced developed earthworm robots. Next, a single unit of the propulsion unit with a pantograph mechanism was developed to meet the requirements of the excavation unit, and it was tested to measure performance in several conditions and environments. The subunit has a large area to contact with the wall of hole, and a space in the middle for an excavation unit. It also showed great performance.

**Chapter 7: Development of a Subsurface Explorer**

This chapter presented the subsurface explorer with connected propulsion and excavation units. The propulsion velocity was modelled and evaluated with an experiment in a pipe. The robot moves at a velocity the same as the model. Finally, excavation experiments were conducted from a launcher as explained for the future mission (Chapter 4). It also showed great performance. It can excavate at the same depth (430 mm) regardless of the weight of the robot, deeper than the excavation unit alone (220 mm), which proves the possibility of use in a lighter gravity condition such as the Moon or Mars. Furthermore, excavation experiments were reported after a depth of the discharged ports reached soil level, now getting rid of the excavated soil using a dust collector. The robot could excavated (650 mm) deeper than the ports reached soil level. It was believed that it could easily excavate deeper if the discharging process were improved, because the velocity did not get slower.

**Chapter 8: Development of a Discharging Part**

To address the issue of discharging for deep excavation, a discharging part was developed. Experiments inside a launcher and soil showed the discharging part successfully winched a bucket

with discharged soil and rarely stopped. The winching number and soil dropped rate were also measured. Excavation experiments with the propulsion and excavation unit were conducted, which succeeded in excavating to a depth of approximately 600 mm, deeper than the discharged ports reached soil level (430 mm). However, it stopped excavating, probably because of the dropped soil that covers between the EA and the bucket.

**Chapter 9: Fundamental Experiments for Modelling the Cutting Resistance**

For modelling the cutting resistance, cutting experiments with the earth auger were conducted in this chapter. The purpose and definition of cutting resistance were explained. In experiments, the effect was classified: pushing force and cutting depth on the screw part, and that on the fish tail. The monitored and measured values were torque and vertical force by a 6 axis sensor. It was found that pushing force mainly affects cutting resistance. The effect of the fish tail part must also be taken into consideration regarding cutting resistance. The excavation performance was evaluated using mechanical specific energy. It reveals a small pushing force consumes little energy with slow excavation, whereas a large pushing force consumes a lot of energy with fast excavation. An advantage of this robot is the pushing force is controllable, which is useful for aerospace exploring purpose.

## 10.2 Future Work

The cutting model will be improved to acquire the requirement torque in various propulsion and excavation conditions and environment of the surrounding materials. The developed subsurface robot will conduct excavation experiments in lunar regolith and martian simulant. It would also test excavation in other materials such as sand, desert, and rock for other applications. An excavation model would be further improved to adapt to conditions and materials as introduced.

The developed robot is not equipped with devices e.g. sampler, seismometer and heat probe. It has some space in a skirt part which can be used to attach a sampler and seismometer. A heat probe is usually set away from a device and robot that generate hinder the measurement. Therefore, a particular method or mechanism would be required for it. First, the robot would be improved to mount a sampler and seismometer.

Strategies and mechanisms for changing excavation direction would be invented. A propulsion unit constituted of a parallel link mechanism [85] which moves in three-dimensions is one of the ideas to achieve. The developed robot with three subunits could move up and down using the peristaltic crawling in a perforated soil. A transport part of an earth auger is required to be bended allowing the three-dimensions movement of the propulsion unit to smoothly move and.

There is need of a robot that can excavate in a horizontal direction in small size for example, analysis of the soil, extraction of gas and oil. The peristaltic crawling robot would be tested in horizontal excavation.

# Appendix A: Characteristic of the Moon

## A1 Physical Properties of the Moon

Table A.1 illustrates the physical properties of the Moon in comparison to the Earth [5]. The gravity of the Moon, 1/6 of that of the Earth is commonly known. Other properties such as temperature and atmosphere on the Moon are wildly different from on the Earth. It is an extremely harsh condition. A robot for a future mission needs protection from that condition and a protection from radiation because of lack of atmosphere.

Table A.1 Physical comparison of the Moon and Earth [5]

| Properties | Moon | Earth |
|---|---|---|
| Gravity at equator [$m/s^2$] | 1.62 | 9.81 |
| Mean surface temperature [°C] | Day: 107<br>Night: -153 | 22 |
| Temperature extremes [°C] | -233 (?) ─ 123 | -89 ─ 58 |
| Atmosphere [$molecules/cm^3$] | Day: ~$10^4$<br>Night: $2 \times 10^5$ | $2.5 \times 10^{19}$ |
| Heat flow (average) [$mW/m^2$] | ~29 | 63 |
| Seismic energy [J/yr] | $2 \times 10^{10}$ (or $10^{14}$) | $10^{17}$ ─ $10^{18}$ |
| Magnetic field [A/m] | 0 (small paleofield) | 24 ─ 56 |

# A2 Lunar Regolith

## A2.1 Lunar Regolith

Regolith is defined as “a general term for the layer or mantle of fragmental and unconsolidated rock material, whether residual or transported and of highly varied character, that nearly everywhere forms the surface of the land and overlies or covers bedrock. It includes rock debris of all kinds, volcanic ash, glacial drift, alluvium, loess and eolian deposits, vegetal accumulations, and soil”.

Regolith covers the Moon surface. Its thickness may not exceed 20 m [5]. The thickness depends on the place. The regolith is generally about 4−5 m thick in the mare areas, and averages about 10−15 m in older highland regions.

## A2.2 Sampled Regolith

Fig. A.1 shows the spots where landers crashed or landed on the Moon surface [5]. The names marked in red conducted sample return or soil mechanics studies corresponding to Table 1.1. Most data on lunar regolith (>90%) have been obtained from the <1 mm fractions.

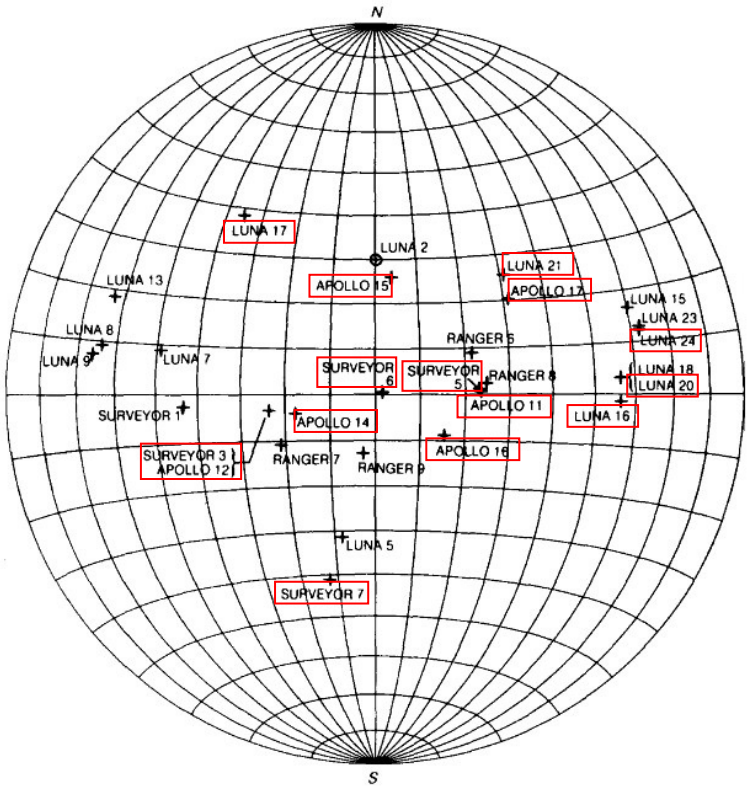


Fig. A2.1 Landing spots [5]

### A2.3 Bulk Density and Relative Density

Bulk density of material is different from the condition such as depth. These data shown in Fig. A.2 were surmized [5]. Calculated values against depth are shown Table A.2. In order to compare with reddish soil and Lunarlant, maximum and minimum bulk density were measured following the regulation [92]. Table A.3 shows the measured values. The maximum bulk density of reddish soil is smaller than Lunarlant and lunar soil. It is thought to be because the range of particle size of reddish soil is narrow, (Fig.5.16); because the size of the soil particles are similar to each other, the density does not become large.

Relative density is the ratio of the difference between the void ratios in its loosest state and existing natural state to the difference between its void ratio in the loosest and densest states. The relative density *Dr* is give as follows:

$$D_r = \frac{e_{Max} - e}{e_{Max} - e_{\min}} \qquad \text{(A.1)}$$

Where $e$ is the void ratio of existing natural state, $e_{Max}$ is the maximum void ratio and

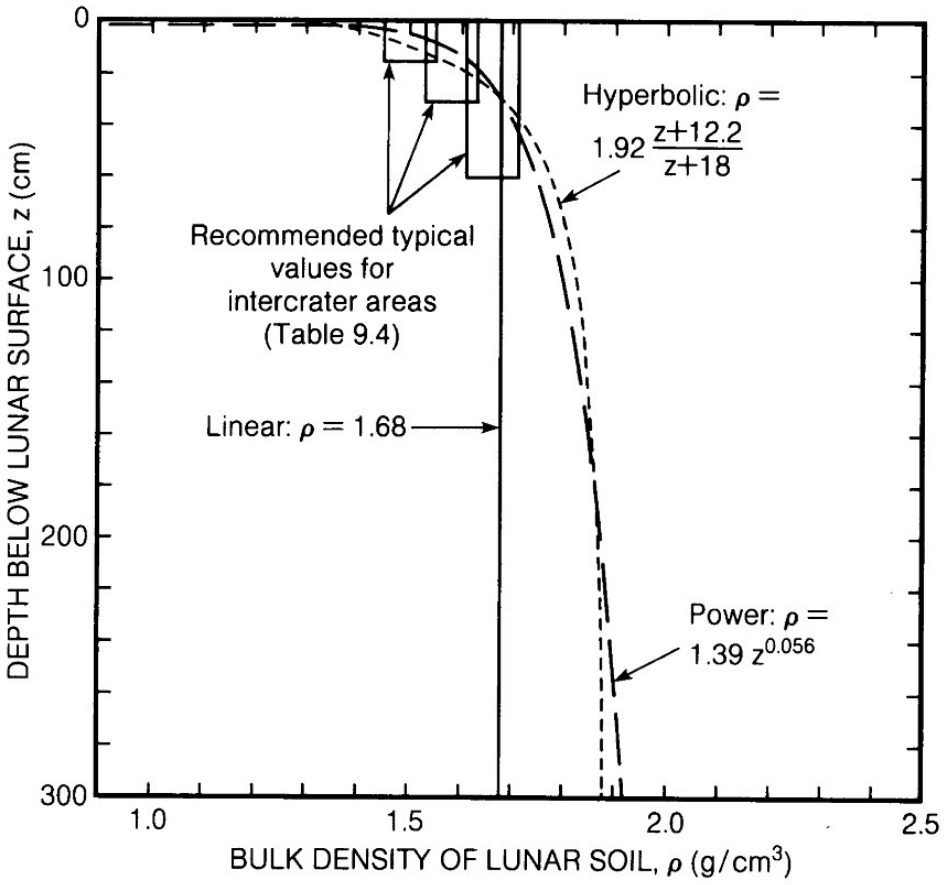


Fig. A.2 Calculated *in situ* bulk density [5]

$e_{min}$ is the minimum void ratio. This formula is also expressed as follows:

$$D_r = \frac{\rho_{Max}}{\rho} \times \frac{\rho - \rho_{\min}}{\rho_{Max} - \rho_{\min}} \qquad \text{(A.2)}$$

Relative density based on returned core samples were calculated assuming $\rho_{min}$ (1.15 g/cm$^3$) and $\rho_{Max}$ (1.82 g/cm$^3$) [5]. Relative density in the top 150 mm is 63%, 84% in the top 30 mm and 97% for the next 350 mm. This indicates that lunar soil becomes very dense at not deep depth.

Table A.2 Bulk density of lunar soil [5]

| Depth range [cm] | Av. density [g/cm3] |
|---|---|
| 0 − 15 | 1.50 ± 0.05 |
| 0 − 30 | 1.58 ± 0.05 |
| 30 − 60 | 1.74 ± 0.05 |
| 0 − 60 | 1.66 ± 0.05 |

Table A.3 Bulk density of red soil and Lunarlant

| | | Red soil | Lunarlant |
|---|---|---|---|
| Density [g/cm$^3$] | Max. | 1.1 | 1.804 |
| | Min. | 0.792 | 1.225 |

# References


[1] Image of the Day Gallery, Sputnik 1, NASA, (http://www.nasa.gov/multimedia/imagegallery/image_feature_924.html, accessed on 18 August 2013).

[2] "News of Science," *Science 18 October 1957*: 739–744.

[3] Luna 2, NASA (http://nssdc.gsfc.nasa.gov/nmc/spacecraftDisplay.do?id=1959-014A, accessed on 18 August 2013).

[4] The Launch of Vostok 1, NASA, (http://starchild.gsfc.nasa.gov/Images/StarChild/space_level2/vostok1_big.gif, accessed on 17 March 2014).

[5] G. Heiken, "Lunar Sourcebook: A User's Guide to the Moon," New York: the Press Syndicate of the University of Cambridge, 1991.

[6] Mission Evaluation Team, "Apollo 11 Mission report," Lyndon B. Johnson Space Center, NASA, Houston, TX , Rep. MSC–00171, November 1969.

[7] Mission Evaluation Team, "Apollo 112 Mission report," Lyndon B. Johnson Space Center, NASA, Houston, TX , Rep. MSC–01855, March 1970.

[8] O. G. Morris, "Apollo 17 Mission report," Lyndon B. Johnson Space Center, NASA, Houston, TX , Rep. JSC–07904, Mar. 1973.

[9] B. Harvey, "Soviet and Russian Lunar Exploration," Springer Jointly published with Praxis Publishing, UK, 2007.

[10] Surveyor: Program Results, NASA, SP–184, 1969.

[11] Solar System Exploration, Surveyor 3 on the Moon, Nasa, (http://solarsystem.nasa.gov/multimedia/display.cfm?IM_ID=8463, accessed on 29 September 2013).

[12] L. D. Jaffe, "Lunar Surface Material: Spacecraft Measurements of Density and Strength," *Science*, vol. 164, no. 3887, pp. 1514–1516, June 1969.

[13] G. Heiken, "Lunar Sourcebook: A User's Guide to the Moon." New York: the Press Syndicate of the University of Cambridge, 1991, p. 485.

[14] Luna-24, Russian Space web, (http://www.russianspaceweb.com/luna24.html, accessed on 5 October 2013).

[15] C. Meyer, "Luna 24: Drill Core," Lunar Sample Compendium, 2009, (http://curator.jsc.nasa.gov/lunar/lsc/index.cfm, accessed on 5 October 2013).

[16] R. Welch, D. Limonadi, and R. Manning, "Systems engineering the Curiosity Rover: A retrospective," *2013 8th International Conference on System of Systems Engineering (SoSE)*, pp.70,75, 2–6 June 2013.

[17] NASA Mars Rover Curiosity Drills Second Rock Target, NASA, (http://www.jpl.nasa.gov/news/news.php?release=2013-168, accessed on 1 April 2013).

[18] JAXA, (http://www.jaxa.jp/projects/sat/muses_c/img/photo.jpg, accessed on 17 March 2013).

[19] First analysis of Tiny Particles from Itokawa, JAXA, (http://www.jaxa.jp/article/special/itokawa/bunseki_e.html, accessed on 5 October 2013).

[20] K. Nagao, R. Okazaki, T. Nakamura, Y. N. Miura, T. Osawa, et al., "Irradiation History of Itokawa Regolith Material Deduced from Noble Gases in the Hayabusa Samples," *Science 26 August 2011*, vol. 333, no. 6046, pp. 1128-1131.

[21] T. Noguchi, T. Nakamura, M. Kimura, M. E. Zolensky, M. Tanaka, et al., "Incipient Space Weathering Observed on the Surface of Itokawa Dust Particles," *Science 26 August 2011*, vol. 333, no. 6046, pp. 1121-1125.

[22] ISECG Posts Update to the Global Exploration Roadmap, ISECG, (https://www.globalspaceexploration.org/c/document_library/get_file?uuid=6bdce6a3-1400-4b47-b6ba-3556755273c3&groupId=10812, accessed on 11 November 2013).

[23] Image of an excavator with bucket, (http://www.aggman.com/files/2010/06/RO51-Komatsu1.jpg, accessed on 5 October 2013).

[24] Image of a boring machine, (http://www.kanto-geo.or.jp/Archive/html/member02/m-html/029.htm, accessed on 5 October 2013).

[25] Image of a shield machine, (http://www.mhi.co.jp/en/news/sec1/1001_w.html, accessed on 5 October 2013).

[26] M. Suparna, P. Bartlett, B. J. Glass, Guerrero, and S. Stanley, "Technologies for Exploring the Martian Subsurface," *2006 IEEE Aerospace Conference*, pp.1–11.

[27] E. Allouis, T. Jorden, N. Patel, S. Senese, P. Magnani, R. Spörri, K. Kapellos, R Wiesendanger, and G. Visentin, "End-to-end Design of a Robotic System for Collecting and Transferring Samples on Mars," in *Proceedings of International Symposium on Artificial Intelligence*, Robotics and Automation in Space Sapporo, August - September , 2010,Japan. pp. 178–185.

[28] H. Shiraishi, S. Tanaka, A. Fujimura, and H. Hayakawa, "The present status of the Japanese penetrator mission: LUNAR-A," *Advances in Space Research*, vol. 42, no. 2, pp. 386–393, Jul. 2008.

[29] Y. Gao, A. Phipps, M. Taylor, I. A. Crawford, A. J. Ball, L. Wilson, D. Parker, M. Sweeting, A. D. S. Curiel, P. Davies, A. Baker, W. T. Pike, A. Smith, and R. Gowen, "Lunar science with affordable small spacecraft technologies: MoonLITE and Moonraker," *Planetary and Space Science*, vol. 56, pp. 368–377, 2008.

[30] Y. Gao, A. Ellery, M. Jaddou, J. Vincent, and S. Eckersley, "Planetary Micro-Penetrator Concept Study with Biomimetric Drill and Sampler Design," *IEEE Transactions on Aerospace and Electronic Systems*, vol. 43, no. 3, pp. 875–885, Jul. 2007.

[31] K. Watanabe, T. Shimoda, T. Kubota, and A. Nakatani, "A Mole-Type Drilling Robot for Lunar Subsurface Exploration," in *Proceedings of 7th International Symposium on Artificial Intelligence, Robotics and Automation in Space*, AS–7, 2003.

[32] K. Nagaoka, T. Kubota, M. Otsuki, and S. Tanaka, “Experimental analysis of a screw drilling mechanism for lunar robotic subsurface exploration,” *Advanced Robotics*, vol. 24, nos. 8–9, pp. 1127–1147, 2010.

[33] V. V Gromov, A. V. Misckevich, and E. N. Yudkin, “The Mobile Penetrometer, A “MOLE” for Sub-Surface Soil Investigation,” in *Proceedings 7th European Space Mechanisms & Tribology Symposium*, Noordwijk, The Netherlands, pp. 151–156,October 1997.

[34] L. Richter, P. Coste, V Gromov, H. Kochan, S. Pinna, and H.-E. Richter, “Development of the “Planetary Underground Tool” Subsurface Soil Sampler for the Mars Express “Beagle 2” Lander,” *Advances in Space Research*, vol. 28, issue 8, pp. 1225–1230, 2001.

[35] L. Richter, P. Coste, V Gromov, H. Kochan, R. Nadalini, T.C. Ng, S. Pinna H.-E. Richter, and K.L. Yung “Development and testing of subsurface sampling devices for the Beagle 2 lander,” *Planetary and Space Science*, vol. 50, issue 9, p. 903-913, 2002.

[36] L. Richter, P. Coste, V. V Gromov, and A. Grzesik, “The Mole with Sampling Mechanism (MSM)- Technology Development and Payload of Beagle 2 Mars Lander,” in *Proceedings of 8th ESA Workshop on Advanced Space Technologies for Robotics and Automation (ASTRA 2004)*, Noordwijk, The Netherlands, November 2004, pp. 2–4.

[37] A. S. Fukunaga, J. M. Morookian, K. Quilin, A. Stoics, and S. Thakoor, “Earthwormlike Exploratory Robots,” NASA Tech Brief, Volume 22. No. 6, No. 138, 1998.

[38] S. Thakoor, B. Kennedy, and A. P. Thakoor, “Insectile and vermform exploratory robots,” NASA Tech Brief, Volume 23. No. 11, 2038, 1999

[39] H. Kudo, and K. Yoshida, “Basic examen by mole-type moon excavation robot,” (in Japanese), in *Proceedings 183rd Conference of the Society of Instrument and Control Engineers*, No. 183–6, 1999.

[40] K. Yoshida, T. Kudo, Y. Kawakatsu, T. Yokoyama, and M. Sonoyama, “Development of a Mole-like Robot for Lunar Subserface Exploration,” (in Japanese), in *Proceedings of 2000, JSME Conference on Robotics and Mechatronics*, Tsukuba, Japan, 2013, 1P1–07.

[41] N. Mizuno, and K. Yoshida, “Development of a Robot Prototype for Excavation and Exploration of the Moon and Planet,” in *Proceedings 183rd Conference of the Society of Instrument and Control Engineers*, pp. 1–8, 2001.

[42] K. Yoshida, N. Mizuno, T. Yokoyama, H. Kanamori M. Sonoyama, and T. Watabe, “Development of a Mole-type Robot for Lunar/Planetary Sub-Surface Exploration, and its Performance Evaluation,” (in Japanese), in *Proceedings of 20th Annual Conference of the Robotics Society of Japan*, Osaka, Japan, 2002, 1J35.

[43] C. R. Stoker, L. Richter, W. H. Smith, L. G. Lemke, P. Hammer, J. B. Dalton, B. Glass, and A. Zent, “The Mars Underground Mole (MUM): A Subsurface Penetration Device with In Situ Infrared Reflectance and Raman Spectroscopic Sensing Capability,” in *Proceedings of*

*6th International Conference on Mars*, California, 3007, 2003.

[44] C. R. Stoker, A. Gonzales, and J. R. Zavaleta, "Moon/Mars Underground Mole," in *Proceedings of the NASA Science and Technology Conference*, Adelphi, MD, 2007.

[45] S. Shimoda, T. Kubota, and I. Nakatani, "A Mole-Type Drilling Robot for Lunar Subsurface Exploration," in *Proceedings of 7th International Symposium on Artificial Intelligence, Robotics and Automation in Space*, pp. 111–115, 2003.

[46] I. Nakatani, I. Nakatani, and T. Kubota, "Study on Mole-Typed Deep Driller Robot for Subsurface Exploration," in *Proceedings of 2005 IEEE International Conference on Robotics and Automation*, pp. 1309–1314, 2003.

[47] T. Kubota, K. Nagaoka, S. Tanaka, and T. Nakamura, "Earthworm Typed Drilling Robot for Subsurface Planetary Exploration," in *Proceedings of IEEE International Conference on Robotics and Biomimetics*, Sanya, China, Dec. 2007, pp. 1394–1399.

[48] S. P. Gorevan, T. M. Myrick, C. Batting, S. Mukherjee, P. Bartlett, and J. Wilson, "Strategies for future mars exploration: An infrastructure for the near and longer-term future exploration of the subsurface of mars," presented at *the 6th International Conference Mars*, Pasadena, CA, 2003.

[49] S. P. Gorevan, K. Y. Kong, T. M. Myrick, P. W. Bartlett, S. Singh, S. Stroescu, Roopnarine, and S. Rafeek, "An Inchworm Deep Drilling System for Kilometer Scale Subsurface Exploration of Mars (IDDS) ," *Forum on Innovative Approaches to Outer Planetary*, January, pp. 1394–1399, 2004.

[50] Y. Liu and B. Weinberg, "Mechanical Design and Modelling of a Robotic Planetary Drilling System," in *Proceedings of ASME International Design Engineering Technical Conferences and Computers and Information Engineering Conference*, Philadelphia, PA, pp. 925–932, 2006.

[51] H. Rabia, "Specific energy as a criterion for drill performance prediction," *International Journal of Rock Mechanics and Mining Sciences & Geomechanics Abstracts*, vol. 19, pp. 39–42, 1982.

[52] K. Nagaoka, M. Otsuki, and S. Tanaka, "Experimental Study on Autonomous Burrowing Screw Robot for Subsurface Exploration on the Moon," *2008 IEEE/RSJ International Conference on Intelligent Robots and Systems*, Nice France, pp. 4105–4109, 2008.

[53] K. Nagaoka, M. Otsuki, and S. Tanaka, "Robotic Screw Explorer for Lunar Subsurface Investigation: Dynamics Modelling and Experimental Validation," *2009 International Conference on Advanced Robotics*, pp. 1–6, 2009.

[54] K. Nagaoka, M. Otsuki, and S. Tanaka, "Experimental Analysis of a Screw Drilling Mechanism for Lunar Robotic Subsurface Exploration," *Advanced Robotics*, vol. 24, no. 8–9, pp. 1127–1147, 2010.

[55] S. Yasuda, and K. Komatsu, “Regolith Drilling Mechanism Using Reaction Torque,” (in Japanese) in *Proceedings of 2008 JSME Conference on Robotics and Mechatronics*, Nagano, Japan, 2P2–A20, 2008.

[56] S. Yasuda, and K. Komatsu, “Research for Regolith Drilling Mechanism Using Reactive Torque,” (in Japanese) in *Proceedings of 18th Space Engineering Conference*, Tokyo, Japan, pp. 75–79, 2010.

[57] S. Yasuda, K. Komatsu, and S. Tanaka, “Research of Self-Turning Screw Mechanism for Lunar/Planetary Exploration,” (in Japanese) in *Proceedings of 2008 JSME Conference on Robotics and Mechatronics*, Nagano, Japan, 1A2–K04, 2011.

[58] S. Yasuda, K. Komatsu, and S. Tanaka, “Self-Turning Screw Mechanism for Burying Geophysical Sensors under Regolith,” in *Proceedings of International Symposium on Artificial Intelligence, Robotics and Automation in Space*, Turin, Italy, 09B02, 2012.

[59] S. Yasuda, K. Komatsu, and S. Tanaka, “Self-Turning Screw Mechanism for Burying Geophysical Sensors under Regolith,” (in Japanese) in *Proceedings of 2008 JSME Conference on Robotics and Mechatronics*, Tsukuba, Japan, 2P1–M01, 2013.

[60] R. Abe, Y. Kawamura, K. Kamijima, and K. Murakami, “Performance Evaluation of Contra-Rotating Drill for DIGBOT,” in *Proceedings of SICE Annual Conference 2010*, Taipei, Taiwan, pp. 885–888, 2010.

[61] C. Boyles, E. Eledui, B. Grasse, J. Johnson, J. B. Long, and N. Toy, “Lunar Wormbot: Design and Development of a Ground Based Robotic Tunneling Worm for Operation in Harsh Environments,” *2011 ESMD Systems Engineering Paper Competition*, pp. 1–62, 2011.

[62] R. A. Russell, “CRABOT: A Biomimetic Burrowing Robot Designed for Underground Chemical Source Location,” *Advanced Robotics*, vol. 25, no. 1–2, pp. 119–134, 2011.

[63] K. Zacny, G. Paulsen, Y. B- Cohen, L. Beegle, S. Sherrit, M. Badescu, B. Mellerowicz, O. Rzepiejewska, J. Craft, S. Sadick, F. Corsetti, Y. Ibarra, X. Bao, H. J. Lee, and B. Abbey, “Wireline Deep Drill for Exploration of Mars, Europa, and Enceladus,” *2013 IEEE Aerospace Conference*, MT, pp. 1–14.

[64] K. Nagaoka, “Study on Soil-Screw Interaction of Exploration Robot for Surface and Subsurface Locomotion in Soft Terrain,” Doctoral Thesis, The Graduate university for Advanced Studies, Japan, p. 85, 2011.

[65] R. McNeill. Alexander, “Exploring Biomechanics, Animals in Motion,” W.H. Freeman and Company, 1992, pp.77–79.

[66] H. Sugi, “Evolution of muscle motion,” (in Japanese), The University of Tokyo Press, p. 72, 1977.

[67] H. Omori, T. Nakamura, T. Yada, T. Murakami, H. Nagai, and T. Kubota, “Excavation mechanism for a planetary underground explorer robot,” in *Proceedings of International*

*Symposium on Robotics*, Munich, Germany, 2010, pp. 1273–1279.

[68] H. Omori, T. Nakamura, T. Murakami, H. Nagai, and T. Kubota, "An earth auger as excavation part for a planetary underground explorer robot using peristaltic crawling," in *Proceedings of International Symposium on Artificial Intelligence, Robotics and Automation in Space*, Sapporo, Japan, 2010, pp. 784–789.

[69] A. Kato, "Excavating machines and particular kind of excavation," Japan Society of Civil Engineers, pp. 73–78, 1979.

[70] Carrier, W. David, III, "Lunar soil grain size distribution," The moon, Springer, Volume 6, Issue 3–4, pp 250–263. 1973.

[71] Graf, J. C. (1993). ''Lunar soils grain size catalog.'' NASA Reference Publication No. 1265.

[72] Carrier, W. David, III, "Particle Size Distribution of Lunar soil", *Journal of Geotechnical and Geoenvironmental Engineering*, Volume 129, No. 10, October 2003, pp 956–959.

[73] Lunarlant, Wel research, (http://www.wel.co.jp/product.html, accessed on 12 October 20 13).

[74] Test Method for Particle Size Distribution of Soils, (in Japanese), The Japanese Geotechnical Society, JGS 0131-2008, 2008.

[75] Practice for Preparing Disturbed Soil Samples for Soil Testing, (in Japanese), JGS 0101-2000, 2000.

[76] Test Method for Density of Soil Particles, (in Japanese), JGS 0111-2000, 2000.

[77] Test Method for Water Content of Soils, (in Japanese), JGS 1203-2000, 2000.

[78] Test Method for Liquid Limit and Plastic Limit of Soils, (in Japanese), JGS 0141-2008, 2008.

[79] Test Method for Maximum and Minimum Densities of Sands, (in Japanese), JGS 0161-2008, 2008.

[80] M. Takahashi, I. Hayashi, N. Iwatsuki, K. Suzumori, and N. Ohki, "The Development of an In-Pipe Microrobot Applying the Motion of an Earthworm," in *Proceedings of 5th International Symposium on Micro Machine and Human Science*, Nagoya, Japan, pp.35–40, 2–4 October 1994.

[81] A. Menciassi, S. Gorini, G. Pernorio, and P. Dario, "A SMA actuated artificial earthworm," in *Proceedings of International Conference on Robotics and Automation*, New Orleans, LA, pp. 3282–3287, 26 April – 1 May 2004.

[82] N. Saga, and T. Nakamura, "Development of a peristaltic crawling robot using magnetic fluid on the basis of the locomotion mechanism of the earthworm, " *Smart Material* and *Structures*, vol. 13, pp.566–569, 2004.

[83] T. Yanagida, K. Adachi, M. Yokojima, and T. Nakamura, "Development of a peristaltic crawling robot attached to a large intestine endoscope using bellows - type artificial rubber muscles," *2012 IEEE/RSJ International Conference on Intelligent Robots and Systems*,

Algarve, Portugal, pp.2935–2940, 7–12 Oct. 2012.

[84] E. V. Mangan, D. A. Kingsley, R. D. Quinn, and H. J. Chiel, "Development of a Peristaltic Endoscope," *2012 IEEE/RSJ International Congress on Robotics and Automation,* Washington, DC, pp.347–352, May 2002.

[85] H. Omori, T. Nakamura, and T. Yada, "An underground explorer robot based on peristaltic crawling of earthworms," *Industrial Robot:, An International Journal*, vol. 36, no. 4, pp. 358–364, 2009.

[86] R.C. Pessier, and M.J. Fear, "Quantifying Common Drilling Problems With Mechanical Specific Energy and a Bit-Specific Coefficient of Sliding Friction, " in *Proceedings of SPE 67th Annual Technical Conf. and Exhibition*, Washington, DC, 24584, 1992.

[87] K. Skonieczny, M.E. DiGioia, R.L. Barsa, D.S. Wettergreen, and W.L. Whittaker, "Configuring innovative regolith moving techniques for lunar outposts," in *Proceedings of 2009 IEEE Aerospace conference*, pp.1–11, March 2009.

[88] B. Rashidi, G. Hareland, and R. Nygaard, "Real-Time Drill Bit Wear Prediction by Combining Rock Energy and Drilling Strength Concepts," in *Proceedings of International Petroleum Exhibition and Conference*, Abu Dhabi, UAE, 117109, November, 2008.

[89] G. Paulsen, K. Zancy, M. Maksymuk, J. Wilson, E. Mumm, J. Craft, K. Davis, and N. Kumar, "Drilling in Ice Bound Lunar Regolith Simulant," in *Proceedings of 40th Lunar and Planetary Science Conference*, Texas, 1138, March, 2009.

[90] M. Bevilacqua1, F. E. Ciarapica, and B. Marchetti, "Acquisition, Processing and Evaluation of Down Hole Data for Monitoring Efficiency of Drilling Processes" *Journal of Petroleum Science Research (JPSR)*, Volume 2, Issue 2, April 2013.

[91] J. Parada, X. Feng, E. Hauerhof, R. Suzuki, and U. Abubakar, "The Deep Sea Energy Park: Harvesting Hydrothermal Energy for Seabed Exploration," University of Southhampton, UK, 2012. p. 60.

# Appendix

[92] R. L. Bates, and J. A. Jackson, "Glossary of Geology," VA: American Geosciences Institute, 1980, p. 543.

# Publications

## Journals

[1] H. Omori, T. Nakamura, and T. Yada, "An underground explorer robot based on peristaltic crawling of earthworms," *An International Journal of Industrial and Service robotics*, *Industrial Robot*, vol. 36 no. 4, pp. 358–364, 2009.

[2] H. Omori, T. Murakami, H. Nagai, T. Nakamura, and T. Kubota, "Development of a Novel Bio-Inspired Planetary Subsurface Explorer: Initial Experimental Study by Prototype Excavator With Propulsion and Excavation Units," *IEEE/ASME Transactions on Mechatronics*, vol. 18, no. 2, pp 459–470, April 2013.

[3] H. Omori, H. Kitamoto, A. Mizushina, T. Nakamura, and T. Kubota, "Development of a Peristaltic Crawling Subsurface Robot for the Moon and Planets -The Effect of Excavation Resistance on the Front Part of the Excavation Unit-," *Journal of Japan Society for Design Engineering, Japan Society for Design Engineering*, (Accepted in October 2013).

## (Co-authored Journal)

[1] H. Kitamoto, H. Omori, H. Nagai, T. Nakamura, H. Osumi, and T. Kubota, "Propulsion Mechanism for a Lunar Subterranean Excavator Using Peristaltic Crawling," *Journal of Robotics and Mechatronics*, vol.25, no.3, pp. 466–475, June 2013.

## Book Chapter

[1] H. Omori, T. Nakamura, T. Iwanaga, and T. Hayakawa, "Development of mobile robots based on peristaltic crawling of an earthworm," in *Robotics 2010: Current and Future Challenges*, 1st edition Vukovar, Croatia: In-Tech, 2010, pp. 299–230.

## Reviewed International Conference Presentations

[1] H. Omori, T. Nakamura, and T. Yada, "Development of an underground explorer robot based on peristaltic crawling of earthworms," in *Proceedings of 11th International Conference on Climbing and Walking Robots and the Support Technologies for Mobile Machine*, Coimbra, Portugal, 2008, pp. 1053–1060.

[2] H. Omori, T. Hayakawa, and T. Nakamura, "Locomotion and Turning Patterns of a Peristaltic Crawling Earthworm Robot Composed of Flexible Units," in *Proceedings of IEEE International Conference on Intelligent Robots and Systems*, Nice, France, 2008, pp. 1630–1635.
[3] H. Omori, T. Nakamura, T. Yada, T. Murakami, H. Nagai, and T. Kubota, "Excavation mechanism for a planetary underground explorer robot," in *Proceedings of International Symposium on Robotics*, Munich, Germany, 2010, pp. 1273–1279.
[4] H. Omori, T. Murakami, H. Nagai, T. Nakamura, and T. Kubota, "An Earth Auger as Excavator for Planetary Underground Explorer Robot Using Peristaltic Crawling," in *Proceedings of International Symposium on Artificial Intelligence, Robotics and Automation in Space*, Sapporo, Japan, 2010, pp. 784–789
[5] H. Omori, T. Murakami, H. Nagai, T. Nakamura, and T. Kubota, "Planetary Subsurface Explorer Robot with Propulsion Units for Peristaltic Crawling," in *Proceedings of International Conference on Robotics and Automation*, Shanghai, China, 2011, pp. 649–654.
[6] H. Omori, T. Murakami, H. Nagai, T. Nakamura, and T. Kubota, "Validation of the measuring condition for a planetary subsurface explorer robot that uses peristaltic crawling," in *Proceedings of 2013 IEEE Aerospace Conference*, Big Sky, MT, 2013, pp. 1–9.
[7] H. Omori, H. Kitamoto, A. Mizushina, T. Nakamura, H. Osumi, and T. Kubota, "Soil cutting experiments and evaluation of an earth auger for a planetary subsurface explorer," in *Proceedings of 2013 6th International Conference on Recent Advances in Space Technologies*, Istanbul, Turkey, 2013, pp. 941–947.
[8] H. Omori, J. -D. Dessimoz, H. Tomori, T. Nakamura, and H. Osumi, "Piaget for the Smart Control of Complex Robotized Applications in Industry," in *Proceedings of 10th International Conference on Informatics in Control, Automation and Robotics*, Reykjavik, Iceland, 2013, vol.2, pp. 528–535.

# (Co-authored Reviewed International Conference Presentations)

[1] H. Nagai, T. Nakamura, H. Omori, and T. Murakami, "Development of an Excavation Robot Based on an Earthworm's Peristaltic Crawling," in *Proceedings of 13th International Conference on Climbing and Walking Robots and the Support Technologies for Mobile Machine*, Nagoya, Japan, 2010, pp. 1089–1096.
[2] A. Yamashita, K. Matsui, R. Kawanishi, T. Kaneko, T. Nakamura, H. Omori, T. Nakamura, H. Asama, "Self-localization and 3-D model construction of pipe by earthworm robot equipped with omni-directional rangefinder," in *Proceedings of 2011 IEEE International Conference on Robotics and Biomimetics*, Phuket, Thailand, 2011, pp. 1017–1023.
[3] H. Kitamoto, H. Omori, H. Nagai, T. Nakamura, H. Osumi, and T. Kubota, "Development of a Propulsion Mechanism for a Lunar Subsurface Excavation Robot with Peristaltic Crawling Mechanism," in *Proceedings of International Symposium on Artificial Intelligence, Robotics and Automation in Space*, Turin, Italy, 2012, 09B–03.
[4] J. -D. Dessimoz, P. -F. Gauthey, and H. Omori, "A Sociology of Intelligent, Autonomous

Cothinkers and Coagents," in *Proceedings of 12th International Conference on Intelligent Autonomous System*, Jeju Island, Korea, 2012.

[5] J. -D. Dessimoz, P. -F. Gauthey, and H. Omori, "Contribution to Social Aspects of Cognition, with Implementation in Signal Supporting Systems and Intelligent Robots, Capable to Interact with Children in the Real-World," *Brain, Mind and Development, 20th World Congress, Social Signal Processing in the International Association for Child and Adolescent Psychiatry and Allied Professions*, Paris, France, 2012. Vol. 60, Bo5S, p.S141.

[6] J. -D. Dessimoz, P. -F. Gauthey, and H. Omori, "Some New Concepts in MCS Ontology for Cognitics; Permanence, Change, Speed, Discontinuity, Innate versus Learned Behavior, and More," *The Fourth International Conference on Advanced Cognitive Technologies and Applications*, Nice, France, 2012.

[7] J. -D. Dessimoz, P. -F. Gauthey, and H. Omori, "Piaget Environment for the Development and Intelligent Control of Mobile, Cooperative Agents and Industrial Robots," in *Proceedings of International Symposium for Robotics*, *International Federation of Robotics*, Taipei, Taiwan, 2012.

[8] A. Mizushina, H. Omori, H. Kitamoto, T. Nakamura, H. Osumi, and T. Kubota, "A discharging mechanism for a lunar subsurface explorer with the peristaltic crawling mechanism," in *Proceedings of 2013 6th International Conference on Recent Advances in Space Technologies*, Istanbul, Turkey, 2013, pp. 955–960.

## Reviewed Domestic Conference Presentations

[1] H. Omori, T. Murakami, H. Nagai, T. Nakamura, and T. Takashi, "Development of a lunar and planetary subsurface explorer robot: Peristaltic crawling robot with a propulsion and excavation mechanism," (in Japanese), in *Proceedings of the 16th Robotics Symposia*, Kagoshima, Japan, 2011, pp. 323–328.

## (Co-authored Reviewed Domestic Conference Presentations)

[1] K. Matsui, R. Kawanishi, A. Yamashita, T. Kaneko, T. Murakami, H. Omori, and T. Nakamura, "Self-Localization and 3-D Model Construction of Pipe by Earthworm Robot Equipped with Omni-Directional Rangefinder," (in Japanese), in *Proceedings of the 16th Robotics Symposia*, Kagoshima, Japan, 2011, pp. 22–29.

## National Domestic Presentations

[1] H. Omori, T. Murakami, H. Nagai, T. Nakamura, and T. Kubota, "Development of a lu nar and planetary subsurface explorer: Development of Prototype Excavator having Prop ulsion and Excavation Units and Excavation Experiments," (in Japanese), in *Proceedings of 2011 JSME Conference on Robotics and Mechatronics*, Okayama, Japan, 2011, 1A2

–K03.

[2] H. Omori, T. Murakami, H. Nagai, T. Nakamura, T. Kubota, and H. Osumi, “月・惑星探査のための蠕動運動型掘削ロボットにおける地中環境計測手法の検討,” (in Japanese), in *Proceedings of the 30th Annual Conference of the Robotics Society of Japan*, Sapporo, Japan, 2012, RSJ2012AC2G3–1.

[3] H. Omori, H. Kitamoto, A. Mizushina, T. Nakamura, H. Osumi, and T. Kubota, “Excavation Evaluation of Excavation Mechanisms for Planetary Underground Explorer Robot,” (in Japanese), in *Proceedings of 2013 JSME Conference on Robotics and Mechatronics*, Tsukuba, Japan, 2013, 2P1–M07.

[4] H. Omori, H. Kitamoto, A. Mizushina, T. Nakamura, and T. Kubota, “Design and Development of Planetary Subsurface Explorer Robot Based on Peristaltic Crawling,” (in Japanese), in *Proceedings of 57th Conference of The Japan Society for Aeronautical and Space Sciences*, Yonago, Japan, 2013, 1J19.

# (Co-authored Domestic Conference Presentations)

[1] T. Yada, H. Omori, and T. Nakamura, “Development of a peristaltic crawling excavation robot for seismometer setting of the moon: Examination of the thrust mechanism in the soil,” (in Japanese), in *Proceedings of the 2008 JSME Conference on Robotics and Mechatronics*, Nagano, Japan, 2008, 2P2–A21.

[2] T. Murakami, H. Omori, T. Yada, and T. Nakamura, “Examination of Excavation Mechanism for a Lunar Underground Explorer Robot using a Peristaltic Crawling,” (in Japanese), in *Proceedings of the 2009 JSME Conference on Robotics and Mechatronics*, Fukuoka, Japan, 2009, 1A2–F15.

[3] H. Nagai, H. Omori, T. Murakami, and T. Nakamura, “Development of peristaltic crawling excavation robot,” (in Japanese), in *Proceedings of the 2010 JSME Conference on Robotics and Mechatronics*, Asahikawa, Japan, 2010, 1A2–B20.

[4] T. Murakami, H. Omori, H. Nagai, and T. Nakamura, “Development of lunar underground explorer robot using peristaltic crawling of earthworm,” (in Japanese), in *Proceedings of the 28th Annual Conference of the Robotics Society of Japan*, Nagoya, Japan, 2010, RSJ2010AC3G2–6.

[5] K. Matsui, A. Yamashita, T. Kaneko, T. Murakami, H. Omori, and T. Nakamura, “3-D Model Construction of Pipe by Earthworm Robot Equipped with Omni-Directional Rangefinder ,” (in Japanese), in *Proceedings of the 28th Annual Conference of the Robotics Society of Japan*, Nagoya, Japan, 2010, RSJ2010AC313–5.

[6] H. Kitamoto, H. Omori, H. Nagai, T. Nakamura, H. Osumi, and T. Kubota, “Developm ent of the excavation robot with the peristaltic motion for investigation of the moon su bsurface,” (in Japanese), in *Proceedings of the 2012 JSME Conference on Robotics and Mechatronics*, Hamamatsu, Japan, 2012, 1A2–L07.

[7] A. Mizushina, H. Omori, H. Kitamoto, T. Nakamura, T. Kubota, and H. Osumi, “Development of a Discharging Unit for a Planetary Subsurface Excavation Robot with Peristaltic Crawling Mechanism,” in *Proceedings of 2013 JSME Conference on Robotics and Mechatronics*, Tsukuba, Japan, 2013, 2P1–M04.

# Patent

[1] 中村太郎，大森隼人，村上太郎，長井　弘明，自動掘削推進装置，特開2011-169056. (in Japanese)

# Awards

[1] Industrial Robot Innovation Award Highly Commended Award, International Conference on Climbing and Walking Robots, September, 2008.
[2] 第26回学員会会長賞, Chuo University, March, 2010.
[3] The Miura Award 2009, The Japan Society of Mechanical Engineers, March, 2010.
[4] Young Investigator Award, Excellent Paper, 57th Conference of The Japan Society for Aeronautical and Space Sciences, December, 2013.

# Acknowledgements

I would like to express my special appreciation and thanks to my advisor Professor Taro Nakamura for his mentorship. He gave me great opportunities not only for research but for research abroad, and domestic and international conferences. His advice on both research as well as on my career have been priceless. I would also like to thank my project members, Mr. Murakami, Mr. Nagai, Mr. Kitamoto, and Ms. Mizushina for working hard and encouraging me at all times. The experiments with soil were difficult, and required mental and physical toughness. Nevertheless, they never gave up following the project. Without their support this dissertation would not have been possible. I would like to offer my special thanks to Professor Osumi, Professor Umeda, and Professor Kunii of Chuo University, for their valuable and constructive suggestions.

I would like to express my very great appreciation to Professor Kubota of the University of Tokyo, for advice and financial support for my project. Advice given by Associate Professor Nagaoka of Tohoku University has been a great help in my project. He worked on an excavation robot for his dissertation which is referred to in my dissertation. I am grateful for support in soil tests and advice in terms of civil engineering given by Professor Kokusho, Mr. Kaneko, Ms. Mukai, and Mr. Koga of Chuo University. I wish to acknowledge advice in civil engineering provided by Professor Kobayashi of the University of Fukui. I would like to express my deep gratitude to Professor Bamford of Bunkyo University for his help with the English in this dissertation and for his advice about writing.

Finally, I wish to thank my family for all their support and encouragement throughout my study.

March. 2014
Hayato Omori